Molecular Biology of the Cell
Vol. 18, 295–312, January 2007

Endocytic Recycling in Yeast Is Regulated by Putative Phospholipid Translocases and the Ypt31p/32p–Rcy1p Pathway[D]

Nobumichi Furuta, Konomi Fujimura-Kamada, Koji Saito, Takaharu Yamamoto, and Kazuma Tanaka

Division of Molecular Interaction, Institute for Genetic Medicine, Hokkaido University Graduate School of Medicine, Sapporo, 060-0815, Japan

Submitted May 26, 2006; Revised October 25, 2006; Accepted October 26, 2006
Monitoring Editor: Sean Munro

Phospholipid translocases (PLTs) have been implicated in the generation of phospholipid asymmetry in membrane bilayers. In budding yeast, putative PLTs are encoded by the *DRS2* gene family of type 4 P-type ATPases. The homologous proteins Cdc50p, Lem3p, and Crf1p are potential noncatalytic subunits of Drs2p, Dnf1p and Dnf2p, and Dnf3p, respectively; these putative heteromeric PLTs share an essential function for cell growth. We constructed temperature-sensitive mutants of *CDC50* in the *lem3*Δ *crf1*Δ background (*cdc50-ts* mutants). Screening for multicopy suppressors of *cdc50-ts* identified *YPT31/32*, two genes that encode Rab family small GTPases that are involved in both the exocytic and endocytic recycling pathways. The *cdc50-ts* mutants did not exhibit major defects in the exocytic pathways, but they did exhibit those in endocytic recycling; large membranous structures containing the vesicle-soluble *N*-ethylmaleimide-sensitive factor attachment protein receptor Snc1p intracellularly accumulated in these mutants. Genetic results suggested that the *YPT31/32* effector *RCY1* and *CDC50* function in the same signaling pathway, and simultaneous overexpression of *CDC50*, *DRS2*, and *GFP-SNC1* restored growth as well as the plasma membrane localization of GFP-Snc1p in the *rcy1*Δ mutant. In addition, Rcy1p coimmunoprecipitated with Cdc50p-Drs2p. We propose that the Ypt31p/32p–Rcy1p pathway regulates putative phospholipid translocases to promote formation of vesicles destined for the *trans*-Golgi network from early endosomes.

INTRODUCTION

Most eukaryotic cells display an asymmetric distribution of phospholipids in the plasma membrane. In general, the aminophospholipids phosphatidylserine (PS) and phosphatidylethanolamine (PE) are enriched in the inner leaflet facing the cytoplasm, whereas phosphatidylcholine (PC), sphingomyelin, and glycolipids are predominantly found in the outer leaflet of the plasma membrane. This lipid asymmetry is generated and maintained by ATP-driven lipid transporters or translocases. The type 4 subfamily of P-type ATPases is implicated in the translocation of phospholipids from the external to the cytosolic leaflet (Graham, 2004; Pomorski *et al*., 2004; Holthuis and Levine, 2005). Five members of this subfamily (Drs2p, Neo1p, Dnf1p, Dnf2p, and Dnf3p) are encoded by the genome of the yeast *Saccharomyces cerevisiae* (Catty *et al*., 1997). Dnf1p and Dnf2p are localized to the plasma membrane, and loss of Dnf1p and Dnf2p abolishes ATP-dependent transport of fluorescently 7-nitrobenz-2-oxa-1,3-diazol-4-yl (NBD)–labeled analogues of PE, PS, and PC from the outer to the inner plasma membrane leaflet (Pomorski *et al*., 2003). Drs2p is localized to endosomes and the *trans*-Golgi network (TGN) (Chen *et al*., 1999; Hua *et al*., 2002; Pomorski *et al*., 2003; Saito *et al*., 2004), suggesting that Drs2p regulates phospholipid asymmetry in these membranes. Moreover, Golgi membranes isolated from a temperature-sensitive *drs2* mutant lacking *DNF1*, *DNF2*, and *DNF3* exhibited defects in the ATP-dependent transport of an NBD-labeled analogue of PS (Natarajan *et al*., 2004). Alder-Baerens *et al*. (2006) also demonstrated that post-Golgi secretory vesicles contained Drs2p- and Dnf3p-dependent NBD-labeled phospholipid translocase activity and that the asymmetric PE arrangement in these vesicles was disrupted in the *drs2*Δ *dnf3*Δ mutant. The *drs2*Δ mutant exhibits TGN defects comparable with those exhibited by strains with clathrin mutations and is defective in the formation of clathrin-coated vesicles (Chen *et al*., 1999; Gall *et al*., 2002). Drs2p is also implicated in endocytic recycling because the exocytic vesicle-soluble *N*-ethylmaleimide-sensitive factor attachment protein receptor (v-SNARE) Snc1p accumulated intracellularly in the *drs2*Δ mutant (Hua *et al*., 2002; Saito *et al*., 2004).

Cdc50p, a conserved integral membrane protein, was identified as a protein required for polarized growth (Misu *et al*., 2003). Cdc50p colocalizes with Drs2p at endosomal

This article was published online ahead of print in *MBC in Press* (http://www.molbiolcell.org/cgi/doi/10.1091/mbc.E06–05–0461) on November 8, 2006.

[D] The online version of this article contains supplemental material at *MBC Online* (http://www.molbiolcell.org).

Address correspondence to: Konomi Fujimura-Kamada (konomi@igm.hokudai.ac.jp) or Kazuma Tanaka (k-tanaka@igm.hokudai.ac.jp).

Abbreviations used: EM, electron microscopy; ER, endoplasmic reticulum; GFP, green fluorescent protein; LAT-A, latrunculin A; mRFP1, monomeric red fluorescent protein 1; PC, phosphatidylcholine; PE, phosphatidylethanolamine; PLT, phospholipid translocase; PS, phosphatidylserine; TGN, *trans*-Golgi network; ts, temperature-sensitive; VPS, vacuolar protein sorting.

and TGN membranes, and it associates with Drs2p as a potential noncatalytic subunit (Saito *et al.*, 2004). In the absence of Cdc50p, Drs2p is retained in the endoplasmic reticulum (ER) and vice versa. In addition to Cdc50p, two Cdc50p-related proteins, Lem3p/Ros3p and Crf1p, are encoded by the yeast genome. Similar to Cdc50p, Lem3p is a potential noncatalytic subunit that associates with Dnf1p (Saito *et al.*, 2004) and Dnf2p (see *Results*), and Crf1p is a potential noncatalytic subunit for Dnf3p (see *Results*). These heteromeric putative phospholipid translocases (PLTs) constitute an essential family for cell growth in which Cdc50p-Drs2p, Lem3p-Dnf1p/2p, and Crf1p-Dnf3p play major, intermediate, and minor roles, respectively (Hua *et al.*, 2002; Saito *et al.*, 2004). The *dnf1*Δ *dnf2*Δ *drs2*Δ mutant exhibits a defect in endocytic internalization at 15°C as assayed by uptake of the endocytic tracer dye *N*-(3-triethylammoniumpropyl)-4-(*p*-diethylaminophenylhexatrienyl) pyridinium dibromide (FM4-64) (see *Materials and Methods*) (Pomorski *et al.*, 2003). The *drs2*Δ *dnf1*Δ mutant exhibits a substantial defect in the transport of alkaline phosphatase to the vacuole (Hua *et al.*, 2002). The *dnf1*Δ *dnf2*Δ *dnf3*Δ mutant intracellularly accumulates Snc1p due to defects in endocytic recycling (Hua *et al.*, 2002). The cellular functions shared by these heteromeric putative PLTs, however, need to be further explored.

In this study, we constructed temperature-sensitive (ts) *cdc50* mutations in a strain lacking *LEM3* and *CRF1*. Screening for multicopy suppressors of the ts growth phenotype identified *YPT32* encoding a Rab family small GTPase, which has been implicated in the formation of exocytic vesicles from the TGN along with its close homologue Ypt31p (Benli *et al.*, 1996; Jedd *et al.*, 1997). The *cdc50-ts lem3*Δ *crf1*Δ mutants, however, did not exhibit major defects in the formation of exocytic vesicles, but instead they exhibited severe defects in endocytic recycling. Interestingly, during the course of this study, it was reported that Ypt31p/32p also regulate endocytic recycling through its effector Rcy1p (Chen *et al.*, 2005). The F-box protein Rcy1p (recycling 1) is involved in recycling out of early endosomes (Wiederkehr *et al.*, 2000). Rcy1p associates with Skp1p, a component of the Skp1p-cullin-F-box protein (SCF) complex but not with other components required for ubiquitin ligase activity, suggesting that Rcy1p regulates endocytic recycling independently of ubiquitination (Galan *et al.*, 2001). The *rcy1*Δ mutant accumulates large membranous structures that seem to be swollen early endosomes (Wiederkehr *et al.*, 2000) and similar structures accumulated in the *cdc50-ts lem3*Δ *crf1*Δ mutants. Simultaneous overexpression of Cdc50p-Drs2p and GFP-Snc1p suppressed the defects in endocytic recycling of the *rcy1*Δ mutant, and Rcy1p was coimmunoprecipitated with Cdc50p and Drs2p. We propose that heteromeric putative PLTs cooperate with Ypt31p/32p-Rcy1p in endocytic recycling.

MATERIALS AND METHODS

Media and Genetic Techniques

Unless otherwise specified, strains were grown in rich medium (YPDA: 1% yeast extract [Difco, Detroit, MI], 2% bacto-peptone [Difco], 2% glucose, and 0.01% adenine). Strains carrying plasmids were selected in synthetic medium (SD) containing the required nutritional supplements (Rose *et al.*, 1990). When indicated, 0.5% casamino acids (Difco) were added to the SD media without uracil (SDA-Ura). Phosphate-depleted rich medium contained 1% yeast extract, 2% bacto-peptone, and 4% glucose, and it was depleted of phosphate as described by Rubin (1973). The synthetic minimal (MV) media used for cell labeling were prepared as described previously (Rothblatt and Schekman, 1989). Standard genetic manipulations of yeast were performed as described previously (Guthrie and Fink, 1991). Yeast transformations were performed by the lithium acetate method (Elble, 1992; Gietz and Woods, 2002). *Escherichia coli* strains DH5α and XL1-Blue were used for construction and amplification of plasmids.

Strains and Plasmids

Yeast strains used in this study are listed in Table 1. The *cdc50-ts* strains were constructed as follows. First, random mutations in *CDC50* were introduced by a polymerase chain reaction (PCR)-based method as described previously (Toi *et al.*, 2003) by using the template pKT1262 (YCplac111-CDC50) and the primers CDC50-5′ (5′-AAGTGACGAATGGAATGATC-3′) corresponding to the nucleotide positions −613 to −594 of *CDC50* and CDC50-3′100R (5′-GTCGCACTATTTTCCAAGCG-3′) complementary to the nucleotide positions 110–129 downstream of the *CDC50* stop codon, to generate the ~1.9-kilobase DNA fragment *CDC50**. The marker fragment *His3MX6* cassette flanked by sequences around the 130 base pairs downstream of the *CDC50* stop codon were generated by PCR by using the template pFA6a-His3MX6 (Longtine *et al.*, 1998) and the primers CDC50-3′100F1 (5′-CGCTTGGAAAATAGTGCGACCGGATCCCCGGGTTAATTAA-3′) and CDC50-3′100R1 (5′-TTCTATCATTTCATCATCTAAATGGGAATAGCAAACCCTGGGAGTTCTTTGAATTCGAGCTCGTTTAAAC-3′) to generate CDC50-3′-His3MX6. The underlined sequence within CDC50-3′100F1 corresponds to the nucleotide positions 110-129 downstream of the *CDC50* stop codon, and is complementary to the sequence of CDC50-3′100R; the underlined sequence within CDC50-3′100R1 is complementary to the nucleotide positions 130–179 downstream of the *CDC50* stop codon. Then, a second PCR was performed to connect the marker fragment to the randomly mutagenized *CDC50* fragment, by using *CDC50** and CDC50-3′-His3MX6 as templates and CDC50-5′ and CDC50-3′100R1 as primers. The amplified DNA fragment was introduced into the genome of YKT496 (*MATα lem3*Δ*::TRP1*), and His^+ transformants were selected at 25°C. Of these transformants, 418 clones were streaked on two YPDA plates, one plate of which was incubated at 25°C and the other plate was incubated at 37°C. Fourteen clones, which exhibited mild ts growth phenotypes, were crossed with YKM48 (*MAT***a** *GAL1p-HA-CDC50*::*KanMX6 crf1*Δ::*hphMX3*), and the resulting diploids were sporulated and dissected. The obtained spore clones whose genotypes were *cdc50**::*His3MX6 lem3*Δ::*TRP1 crf1*Δ::*hphMX3* were tested for growth at 25 and 37°C. The two clones (*cdc50-11*::*His3MX6 lem3*Δ::*TRP1 crf1*Δ::*hphMX3* and *cdc50-162*::*His3MX6 lem3*Δ::*TRP1 crf1*Δ::*hphMX3*) that exhibited the tightest ts phenotype were chosen for further analyses.

Yeast strains carrying a complete gene deletion (*CRF1*), enhanced green fluorescent protein (EGFP)-tagged genes (*KEX2*, *VPS10*, *DNF2*, and *DNF3*), 13 x Myc-tagged genes (*CDC50*, *DNF2*, and *DNF3*), the 3 x hemagglutinin (HA)-tagged *CRF1* gene, or the monomeric red fluorescent protein 1 (mRFP1)-tagged *DRS2* gene were constructed by PCR-based procedures as described previously (Longtine *et al.*, 1998). *DNF2-EGFP* was functional, because the *drs2*Δ *dnf3*Δ *DNF2-EGFP* mutant grew at the same rate as the *drs2*Δ *dnf3*Δ *DNF2* mutant at 28°C, at which the *drs2*Δ *dnf3*Δ *dnf2*Δ mutant exhibited a synthetic growth defect (our unpublished data). *DRS2-mRFP1* was functional, because cells harboring the *DRS2-mRFP1* allele instead of the *DRS2* grew normally at 18°C, at which the *drs2*Δ mutant was lethal (our unpublished data). The *rcy1* or *lem3* disruption mutants were constructed on our strain background as follows. The regions containing the disruption marker and the flanking sequences were PCR amplified using genomic DNA derived from the *rcy1*Δ*::KanMX4* or *lem3*Δ*::KanMX4* strain (a gift from C. Boone, University of Toronto, Toronto, Ontario, Canada) as a template. The amplified DNA fragments were then introduced into the appropriate strains. All constructs made by the PCR-based procedure were verified by colony-PCR amplification to confirm that replacement had occurred at the expected loci. The *rcy1*Δ*::hphMX4* strain was constructed by replacing the *KanMX4* cassette of YKT951 (*rcy1*Δ*::KanMX4*) with the *hphMX4* cassette prepared from pAG32 (Goldstein and McCusker, 1999). The *vps1*Δ and *vps4*Δ deletion mutants were gifts from C. Boone, and the *vps30*Δ strain was a gift from Y. Ohsumi (National Institute for Basic Biology, Okazaki, Japan).

The plasmids used in this study are listed in Table 2. The $YPT32^{Q72L}$ and $YPT32^{S27N}$ alleles were made by using a QuikChange site-directed mutagenesis kit (Stratagene, La Jolla, CA) with the plasmid pKT1555 (YEplac181-YPT32). The mutagenic oligonucleotides were YPT32-Q72L-1 (GAT TTG GGA CAC GGC AGG TCT AGA ACG TTA CAG GGC CAT CAC G) and its complement YPT32-Q72L-2 for $YPT32^{Q72L}$ and YPT32-S27N-1 (GAC TCC GGT GTG GGT AAA AAT AAT CTG TTG TCG AGA TTT ACA AC) and its complement YPT32-S27N-2 for $YPT32^{S27N}$. We sequenced the entire open reading frame of *YPT32* in each construct to verify that only the desired substitution was introduced. Epitope-tagged Rcy1 proteins were functional, because both pRS416-*GFP-RCY1* and YEplac195-*HA-BS-RCY1* plasmids suppressed the growth defect of the *rcy1*Δ mutant at 18°C (our unpublished data). Schemes detailing the construction of plasmids are available upon request.

*Isolation of Multicopy Suppressors of the cdc50-ts lem3*Δ *crf1*Δ *Mutants*

The *cdc50-11 lem3*Δ *crf1*Δ (YKT993) and *cdc50-162 lem3*Δ *crf1*Δ (YKT942) strains were transformed with a yeast genomic DNA library constructed in the multicopy plasmid YEp13 (kindly provided by Y. Ohya, University of Tokyo, Tokyo, Japan). After transformation, cells were incubated at 25°C for 24 h to allow recovery and then were incubated at 37°C for 2 d on SD-Leu

Table 1. *S. cerevisiae* strains used in this study

Strain[a]	Genotype	Reference or source
ANS2-3A	*MATα ura3-52 leu2-3, 112 his3 his4 sec2-56*	Gift from A. Nakano
ANS6-2D	*MATα ura3-52 leu2-3, 112 trp1-289 his3 his4 sec6-4*	Gift from A. Nakano
AKY15	*MAT***a** *ade2-101 lys2-801 ura3-52 his3Δ-200 trp1Δ-63 leu2Δ-1 Δpho8::PHO8Δ60 vps30Δ::LEU2*	Kihara *et al*. (2001)
YEF473	*MAT***a**/*α lys2-801/lys2-801 ura3-52/ura3-52 his3Δ-200/his3Δ-200 trp1Δ-63/trp1Δ-63 leu2Δ-1/leu2Δ-1*	Longtine *et al*. (1998)
YKT38	*MAT***a** *lys2-801 ura3-52 his3Δ-200 trp1Δ-63 leu2Δ-1*	Misu *et al*. (2003)
YKT259	*MAT***a** *lys2-801 ura3-52 his3Δ-200 trp1Δ-63 leu2Δ-1 CDC50-EGFP::kanMX6*	Saito *et al*. (2004)
YKT496	*MAT***a** *lys2-801 ura3-52 his3Δ-200 trp1Δ-63 leu2Δ-1 lem3Δ::TRP1*	This study
YKT760	*MATα lys2-801 ura3-52 his3Δ-200 trp1Δ-63 leu2Δ-1 DNF1–13Myc::TRP1*	This study
YKT768	*MATα lys2-801 ura3-52 his3Δ-200 trp1Δ-63 leu2Δ-1 DRS2-EGFP::kanMX6*	Saito *et al*. (2004)
YKT792	*MAT***a** *lys2-801 ura3-52 his3Δ-200 trp1Δ-63 leu2Δ-1 DRS2–13Myc::TRP1*	This study
YKT871	*MAT***a** *lys2-801 ura3-52 his3Δ-200 trp1Δ-63 leu2Δ-1 DRS2-mRFP1::TRP1*	This study
YKT902	*MAT***a** *lys2-801 ura3-52 his3Δ-200 trp1Δ-63 leu2Δ-1 lem3Δ::TRP1 crf1Δ::hphMX3*	This study
YKT903	*MAT***a** *lys2-801 ura3-52 his3Δ-200 trp1Δ-63 leu2Δ-1 KEX2-EGFP::kanMX6*	This study
YKT921	*MATα lys2-801 ura3-52 his3Δ-200 trp1Δ-63 leu2Δ-1 DNF2-EGFP::kanMX6*	This study
YKT923	*MATα lys2-801 ura3-52 his3Δ-200 trp1Δ-63 leu2Δ-1 lem3Δ::TRP1 DNF2-EGFP::kanMX6*	This study
YKT925	*MATα lys2-801 ura3-52 his3Δ-200 trp1Δ-63 leu2Δ-1 DNF3-EGFP::kanMX6*	This study
YKT928	*MATα lys2-801 ura3-52 his3Δ-200 trp1Δ-63 leu2Δ-1 crf1Δ::hphMX3 DNF3-EGFP::kanMX6*	This study
YKT942	*MAT***a** *lys2-801 ura3-52 his3Δ-200 trp1Δ-63 leu2Δ-1 cdc50-162::HIS3MX6 lem3Δ::TRP1 crf1Δ::hphMX3*	This study
YKT949	*MAT***a** *lys2-801 ura3-52 his3Δ-200 trp1Δ-63 leu2Δ-1 dnf1Δ::hphMX3 dnf2Δ::kanMX6 dnf3Δ::HIS3MX6*	This study
YKT951	*MAT***a** *lys2-801 ura3-52 his3Δ-200 trp1Δ-63 leu2Δ-1 rcy1Δ::kanMX4*	This study
YKT957	*MATα lys2-801 ura3-52 his3Δ-200 trp1Δ-63 leu2Δ-1 VPS10-EGFP::kanMX6*	This study
YKT993	*MAT***a** *lys2-801 ura3-52 his3Δ-200 trp1Δ-63 leu2Δ-1 cdc50-11::HIS3MX6 lem3Δ::TRP1 crf1Δ::hphMX3*	This study
YKT994	*MAT***a** *lys2-801 ura3-52 his3Δ-200 trp1Δ-63 leu2Δ-1 cdc50-11::HIS3MX6 lem3Δ::TRP1 crf1Δ::hphMX3 DRS2-EGFP::kanMX6*	This study
YKT1000	*MAT***a** *lys2-801 ura3-52 his3Δ-200 trp1Δ-63 leu2Δ-1 cdc50-11::HIS3MX6 lem3Δ::TRP1 crf1Δ::hphMX3 KEX2-EGFP::kanMX6*	This study
YKT1001	*MAT***a** *lys2-801 ura3-52 his3Δ-200 trp1Δ-63 leu2Δ-1 cdc50-162::HIS3MX6 lem3Δ::TRP1 crf1Δ::hphMX3 KEX2-EGFP::kanMX6*	This study
YKT1004	*MAT***a** *lys2-801 ura3-52 his3Δ-200 trp1Δ-63 leu2Δ-1 cdc50-11::HIS3MX6 lem3Δ::kanMX4 crf1Δ::hphMX3 SEC7-mRFP1::TRP1*	This study
YKT1008[b]	*MATα ura3 his3 trp1 leu2 cdc50-11::HIS3MX6 lem3Δ::TRP1 sec6-4*	This study
YKT1009[b]	*MAT***a** *ura3 his3 trp1 leu2 his4? lem3Δ::TRP1 crf1Δ::hphMX3 sec6-4*	This study
YKT1010[b]	*MATα ura3 his3 trp1 leu2 his4? sec6-4*	This study
YKT1011[b]	*MAT***a** *ura3 his3 trp1 leu2 cdc50-11::HIS3MX6 lem3Δ::TRP1 crf1Δ::hphMX3 sec6-4*	This study
YKT1062	*MATα lys2-801 ura3-52 his3Δ-200 trp1Δ-63 leu2Δ-1 DNF2-13Myc::TRP1*	This study
YKT1086	*MAT***a** *lys2-801 ura3-52 his3Δ-200 trp1Δ-63 leu2Δ-1 cdc50-11::HIS3MX6 lem3Δ::TRP1 crf1Δ::hphMX3 VPS10-EGFP::kanMX6*	This study
YKT1088	*MAT***a** *lys2-801 ura3-52 his3Δ-200 trp1Δ-63 leu2Δ-1 cdc50-162::HIS3MX6 lem3Δ::TRP1 crf1Δ::hphMX3 VPS10-EGFP::kanMX6*	This study
YKT1098	*MATα lys2-801 ura3-52 his3Δ-200 trp1Δ-63 leu2Δ-1 CRF1–3HA::HIS3MX6*	This study
YKT1099	*MATα lys2-801 ura3-52 his3Δ-200 trp1Δ-63 leu2Δ-1 CRF1-3HA::HIS3MX6 DNF2-13Myc::TRP1*	This study
YKT1100	*MATα lys2-801 ura3-52 his3Δ-200 trp1Δ-63 leu2Δ-1 CRF1-3HA::HIS3MX6 DNF3-13Myc::TRP1*	This study
YKT1101	*MATα lys2-801 ura3-52 his3Δ-200 trp1Δ-63 leu2Δ-1 CDC50-13Myc::HIS3MX6*	This study
YKT1102	*MAT***a** *lys2-801 ura3-52 his3Δ-200 trp1Δ-63 leu2Δ-1 rcy1Δ::hphMX4 CDC50-EGFP::kanMX6*	This study
YKT1310	*MAT***a** *lys2-801 ura3-52 his3Δ-200 trp1Δ-63 leu2Δ-1 lem3Δ::TRP1 crf1Δ::hphMX3 KEX2-EGFP::kanMX6*	This study
YNF61	*MAT***a** *lys2-801 ura3-52 his3Δ-200 trp1Δ-63 leu2Δ-1 lem3Δ::TRP1 crf1Δ::hphMX3* [*GFP-SNC1 URA3 CEN*]	Transformant of YKT902 with pRS416 GFP-SNC1
YNF63	*MAT***a** *lys2-801 ura3-52 his3Δ-200 trp1Δ-63 leu2Δ-1* [*GFP-SNC1 URA3 CEN*]	Transformant of YKT38 with pRS416 GFP-SNC1
YNF65	*MAT***a** *lys2-801 ura3-52 his3Δ-200 trp1Δ-63 leu2Δ-1 cdc50-11::HIS3MX6 lem3Δ::TRP1 crf1Δ::hphMX3* [*GFP-SNC1 URA3 CEN*]	Transformant of YKT993 with pRS416 GFP-SNC1
YNF67	*MAT***a** *lys2-801 ura3-52 his3Δ-200 trp1Δ-63 leu2Δ-1 cdc50-162::HIS3MX6 lem3Δ::TRP1 crf1Δ::hphMX3* [*GFP-SNC1 URA3 CEN*]	Transformant of YKT942 with pRS416 GFP-SNC1
YNF153	*MAT***a** *lys2-801 ura3-52 his3Δ-200 trp1Δ-63 leu2Δ-1 cdc50-11::HIS3MX6 lem3Δ::kanMX4 crf1Δ::hphMX3 SEC7-mRFP1::TRP1* [*GFP-SNC1 URA3 CEN*]	Transformant of YKT1004 with pRS416 GFP-SNC1
YNF784	*MAT***a** *lys2-801 ura3-52 his3Δ-200 trp1Δ-63 leu2Δ-1 dnf1Δ::hphMX3 dnf2Δ::kanMX6 dnf3Δ::HIS3MX6* [*GFP-SNC1 URA3 CEN*]	Transformant of YKT949 with pRS416 GFP-SNC1

Continued

Table 1. *Continued*

Strain[a]	Genotype	Reference or source
KKT276	*MAT***a** *lys2Δ0 ura3Δ0 his3Δ1 leu2Δ0 vps1Δ::kanMX4*	Gift from C. Boone
KKT277	*MAT***a** *lys2Δ0 ura3Δ0 his3Δ1 leu2Δ0 vps4Δ::kanMX4*	Gift from C. Boone
YKM48	*MAT***a** *lys2-801 ura3-52 his3Δ-200 trp1Δ-63 leu2Δ-1 GAL1p-HA-CDC50::kanMX6 crf1Δ::hphMX3*	This study

[a] YKT, YNF, and YKM strains are isogenic derivatives of YEF473 except for YKT1008, YKT1009, YKT1010, and YKT1011.

[b] YKT1008 is segregant from a cross of ANS6-2D with YKT993, YKT1009 is segregant from a cross of ANS6-2D with YKT942, YKT1010 is segregant from a cross of ANS6-2D with YKT902, and YKT1011 is segregant from a cross of YKT1008 with YKT1009.

plates. Approximately 63,000 YKT993 transformants and 42,000 YKT942 transformants were screened, and 59 and 54 transformants that reproducibly grew at 37°C were obtained, respectively. The transformants that contained *CDC50* or *CRF1* on the plasmid were identified by colony-PCRs and were eliminated. The strains that contained *LEM3* on the plasmid were identified by the PCR by using total DNA prepared from the rest of the candidate transformants and were eliminated. Plasmids from the remaining eight and four transformants of YKT993 and YKT942, respectively, were further analyzed. Based on restriction mapping, nine of the 12 plasmids were shown to be identical, whereas the other three plasmids were distinct from each other. The four different plasmids were retransformed into YKT993 and YKT942 to confirm their ability to suppress the ts growth phenotypes. Two of the four plasmids exhibited weaker suppression activities and were not further analyzed. The genes contained within the remaining two plasmids were identified by sequencing both ends of the inserts. The two plasmids contained overlapping genomic DNA fragments, and subcloning analysis revealed that the *YPT32* gene was responsible for the suppression activity.

Purification of Secretory Vesicles and Enzyme Assays

Purification of secretory vesicles was performed as described (Harsay and Bretscher, 1995) with minor modifications. Briefly, cells were grown at 25°C to the early to mid-logarithmic phase (OD_{600} of 0.5–0.7) in 1 liter of synthetic medium, harvested by centrifugation, and resuspended in phosphate-depleted rich medium. Growth was continued at 25°C for 90 min to induce acid phosphatase secretion. Cells were then incubated at 37°C for 2 h before harvesting. Cells were converted to spheroplasts and lysed using 20 strokes in a Dounce glass homogenizer with a tight pestle (Wheaton Industries, Millville, NJ) in lysis buffer containing 0.8 M sorbitol, with 10 mM triethanolamine and 1 mM EDTA, adjusted to pH 7.2 with acetic acid (TEA), and protease inhibitors (1 μg/ml aprotinin, 1 μg/ml leupeptin, 1 μg/ml pepstatin, 2 mM benzamidine, and 1 mM phenylmethylsulfonyl fluoride). A 700 × *g* spin for 10 min generated the pellet (P1) and supernatant (S1) fractions. The S1 fraction was spun at 13,000 × *g* for 20 min to generate P2 and S2. The S2 fraction was centrifuged at 100,000 × *g* for 1 h in an SW28 rotor (Beckman Coulter, Fullerton, CA) to generate membrane pellets (P3). P3 membrane pellets were overlaid with 300 μl of 0.8 M sorbitol/TEA and placed on ice for 2–3 h to allow easy resuspension. For gradient fractionation, a 12-ml 15–30% continuous Nycodenz gradient in 0.8 M sorbitol/TEA was created. The P3 membranes were adjusted to 35% Nycodenz in a total volume of 1 ml and loaded into the bottom of the gradient using a 10-cm needle. Gradients were centrifuged in a P40ST rotor (Hitachi, Tokyo, Japan) at 100,000 × *g* for 19 h, and 0.8-ml fractions were manually collected from the top of the samples.

Enzymatic assays for acid phosphatase, exoglucanase, and invertase activities were performed as described previously (Harsay and Bretscher, 1995), except that fractions were not diluted when the invertase activity was measured.

Antibodies

The rabbit anti-Pma1p polyclonal antibodies were gifts from R. Serrano (Polytechnic University of Valencia, Valencia, Spain). The rabbit anti-carboxypeptidase Y (CPY) and anti-invertase polyclonal antibodies were gifts from A. Nakano (RIKEN, Wako, Japan). Rabbit anti-Lem3p polyclonal antibodies were gifts from M. Umeda (Kyoto University, Kyoto, Japan). The mouse anti-HA (HA.11) and anti-myc (9E10) monoclonal antibodies were purchased from BAbCO (Richmond, CA) and Sigma-Aldrich (St. Louis, MO), respectively. The horseradish peroxidase-conjugated secondary antibodies (sheep anti-mouse IgG and donkey anti-rabbit IgG) used for immunoblotting were purchased from GE Healthcare (Little Chalfont, Buckinghamshire, United Kingdom).

Immunoprecipitation Analysis

Immunoprecipitation analysis of Lem3p-Dnf2p and Crf1p-Dnf3p was performed as described previously (Saito *et al.*, 2004). Coimmunoprecipitation analysis of Rcy1p with Cdc50p, Drs2p, Dnf1p, and Dnf2p was similarly performed. Briefly, cells were grown at 30°C to a cell density of 0.5 OD_{600}/ml

Table 2. Plasmids used in this study

Plasmid	Characteristics	Reference or source
pKT1259 [YEplac181 CDC50]	*CDC50 LEU2 2 μm*	Misu *et al.* (2003)
pRS416 GFP-SNC1	P_{TPI1}*-GFP-SNC1 URA3 CEN*	Lewis *et al.* (2000)
pRS416 GFP-SNC1 pm	P_{TPI1}*-GFP-SNC1pm URA3 CEN*	Lewis *et al.* (2000)
pKT1262 [YCplac111 CDC50]	*CDC50 LEU2 CEN*	This study
pKT1472 [YEplac195 DRS2 CDC50]	*DRS2 CDC50 URA3 2 μm*	Saito *et al.* (2004)
pKT1486 [P_{ACT1}- SUC2]	P_{ACT1}*-SUC2 URA3 CEN*	This study
pKT1487 [pRS416 GFP-PEP12]	P_{TPI1}*-GFP-PEP12 URA3 CEN*	This study
pKT1490 [pRS315 GFP-SNC1]	P_{TPI1}*-GFP-SNC1 LEU2 CEN*	This study
pKT1554 [YEplac181 YPT31]	*YPT31 LEU2 2 μm*	This study
pKT1555 [YEplac181 YPT32]	*YPT32 LEU2 2 μm*	This study
pKT1560 [YEplac181 GFP-RCY1]	*GFP-RCY1 LEU2 2 μm*	This study
pKT1563 [pRS416 mRFP-SNC1]	P_{TPI1}*-mRFP1-SNC1 URA3 CEN*	This study
pKT1564 [pRS416 HA-SNC1]	P_{TPI1}*-HA-SNC1 URA3 CEN*	This study
pKT1566 [YEplac181 GFP-TLG1]	*GFP-TLG1 LEU2 2 μm*	This study
pKT1578 [YEplac181 YPT32^{Q72L}]	*YPT32^{Q72L} LEU2 2 μm*	This study
pKT1579 [YEplac181 YPT32^{S27N}]	*YPT32^{S27N} LEU2 2 μm*	This study
pKT1626 [YEplac195 HA-BS-RYC1]	*HA-RCY1 URA3 2 μm*	This study
YEplac181	*LEU2 2 μm*	Gietz and Sugino (1988)
YEplac195	*URA3 2 μm*	Gietz and Sugino (1988)
pRS315	*LEU2 CEN*	Sikorski and Hieter (1989)

in SDA-Ura medium. Cells collected from 400 ml of the cultures were washed twice with ice-cold water and resuspended at 200 OD_{600}/ml in lysis buffer (10 mM Tris-HCl, pH 7.5, 0.3 M sorbitol, 0.1 M NaCl, and 5 mM $MgCl_2$) containing protease inhibitors (1 μg/ml aprotinin, 1 μg/ml leupeptin, 1 μg/ml pepstatin, 2 mM benzamidine, and 1 mM phenylmethylsulfonyl fluoride). The cells were lysed by Multi-beads shocker (Yasui Kikai, Osaka, Japan). Cell lysates were centrifuged at 400 $\times$ *g* for 5 min, and the resulting supernatant was centrifuged at 100,000 $\times$ *g* for 1 h at 4°C. For immunoprecipitation, the pellets were solubilized in 0.8 ml of immunoprecipitation buffer (10 mM Tris-HCl, pH 7.5, 150 mM NaCl, 2 mM EDTA, and 1% 3-[(3-cholamidopropyl)dimethylammonio]propanesulfonate [CHAPS]) containing the above-mentioned protease inhibitors. Insoluble material was removed by centrifugation at 20,630 $\times$ *g* for 5 min at 4°C. The cleared lysates were incubated with 5 μg of anti-Myc antibody for 1 h at 4°C. We then rotated the samples with 20 μl of protein G-Sepharose 4 Fast Flow (GE Healthcare) for 1 h at 4°C. The protein G-Sepharose beads were pelleted and washed three times with immunoprecipitation buffer in the absence of detergents before suspending them in SDS-PAGE sample buffer.

Immunoblotting Analysis

Immunoblotting analysis was performed as described previously (Misu *et al.*, 2003). For SDS-PAGE of Drs2p-Myc, Dnf1p-Myc, Dnf2p-Myc, and Dnf3p-Myc, samples were heated at 37°C for 20 min before loading. For SDS-PAGE of Pma1p, 10-μl aliquots of each fraction from the Nycodenz density gradient fractionation were mixed with 10 μl of 2X SDS-PAGE sample buffer, followed by heating at 37°C for 15 min before loading. Anti-HA, anti-Myc, and anti-Lem3p antibodies were used at a 1:1000 dilution. Anti-Pma1p antibodies were used at a 1:5000 dilution. For the colony blot assay, anti-CPY antibodies were used at a 1:1000 dilution.

Microscopic Observations

Cells were observed using a Nikon ECLIPSE E800 microscope (Nikon Instec, Tokyo, Japan) equipped with an HB-10103AF superhigh-pressure mercury lamp and a 1.4 numerical aperture 100× Plan Apo oil immersion objective lens (Nikon Instec) with appropriate fluorescence filter sets (Nikon Instec) or differential interference contrast optics. Images were acquired using a cooled digital charge-coupled device camera (C4742-95-12NR; Hamamatsu Photonics, Hamamatsu, Japan) and AQUACOSMOS software (Hamamatsu Photonics). Observations are based on the characterization of >100 cells.

To assess the endocytic pathway using the lipophilic styryl dye FM4-64, cells were grown to late-logarithmic phase in YPDA medium at 25°C or 37°C for 3 h. Four OD_{600} units of cells were labeled with 32 μM FM4-64 (Invitrogen, Carlsbad, CA) in 100 μl of YPDA medium for 15 min at 25 or 37°C. Cells were harvested by centrifugation, resuspended in 200 μl of fresh YPDA medium, and chased at 25 or 37°C for 30 min. Cells were washed twice with 100 μl of SD medium and immediately observed using a G-2A filter set. To mark early endosomes with FM4-64, cells were grown to early logarithmic phase in SDA-Ura medium at 25°C and then shifted to 37°C for 3 h. Four OD_{600} units of cells were incubated with 32 μM FM4-64 in 100 μl of YPDA medium on ice for 30 min. Cells were harvested by centrifugation, resuspended in 200 μl of fresh YPDA medium and chased at 37°C for 10 min. After chase, cells were harvested by centrifugation, resuspended in ice-cold SD medium, and immediately observed. To visualize the vacuole lumen, cells were stained with CellTracker Blue CMAC (Invitrogen) according to the manufacturer's protocol and observed using a UV-1A filter set.

Most GFP- or mRFP1-tagged proteins were observed in living cells, which were grown to early to mid-logarithmic phase, harvested, and resuspended in SD medium. Cells were immediately observed using a GFP bandpass (for GFP) or a G2-A (for mRFP1) filter set. Localization of GFP- or mRFP1-tagged proteins was also examined in fixed cells. Fixation was performed for 5 min at 37°C by direct addition of a commercial 37% formaldehyde stock (Wako Pure Chemical Industries, Osaka, Japan) to a final concentration of 0.5% in the medium, followed by a 10-min incubation at 25°C. After fixation, cells were washed twice with phosphate-buffered saline and examined. The cell fixation protocol resulted in images of the GFP- and mRFP1-fusion proteins that were similar to those obtained with living cells (our unpublished observation).

Electron Microscopy (EM)

Ultrastructural observation of cells by conventional EM was performed using the glutaraldehyde-permanganate fixation technique (Kaiser and Schekman, 1990). Cells were embedded in Spurr's resin (Nissin EM, Tokyo, Japan). Thin sections (50–60 nm) were cut on an Ultracut microtome (Leica, Wetzlar, Germany) equipped with a Sumiknife (Sumitomo Electric Industries, Osaka, Japan), stained with 3% uranyl acetate and Reynold's lead citrate, and viewed using an H-7100 electron microscope (Hitachi) at 75 kV. Immuno-EM was performed using the aldehyde fixation/metaperiodate permeabilization method (Mulholland and Botstein, 2002), except that glutaraldehyde was not included in the fixative. Cells were embedded in LR White resin (medium grade; London Resin Company, Berkshire, United Kingdom) and sectioned as described above. Mouse anti-HA antibody (HA.11) was used as a primary antibody at a 1:500 dilution. Ten-nanometer gold-conjugated anti-mouse IgG antibodies (BBInternational, Cardiff, United Kingdom) were preadsorbed with fixed wild-type cells and used as secondary antibodies at a 1:100 dilution. Samples were poststained with uranyl acetate and viewed as described above.

^{35}S Pulse-Chase and Immunoprecipitation Experiments

Metabolic labeling of yeast cells, preparation of cell extracts, and immunoprecipitation were performed essentially as described previously (Rothblatt and Schekman, 1989; Gaynor *et al.*, 1994; Yahara *et al.*, 2001). To visualize target proteins, total proteins or immunoprecipitated proteins were resolved by SDS-PAGE followed by analysis using a FLA3000 fluorescent image analyzer (Fuji Photo Film, Tokyo, Japan).

To assay internal and external invertase, cells were grown to mid-logarithmic phase in MV-low sulfate medium containing 5% glucose at 37°C for 2 h. Three (labeled for 7 min) or five (labeled for 2 min) OD_{600} units of cells were collected, converted to spheroplasts with Zymolyase 100T (25 U/ml cell suspension; Seikagaku Kogyo, Tokyo, Japan), and incubated at 37°C for 30 min. Spheroplasts were resuspended in MV-no sulfate medium containing 1 M sorbitol and 0.1% glucose, grown at 37°C for 30 min, and labeled with 50 μCi of Tran^{35}S-label (PerkinElmer Life and Analytical Sciences, Boston, MA) per OD_{600} unit of cells for 7 or 2 min. A chase was initiated by adding a chase solution (MV-no sulfate medium with 4 mM ammonium sulfate, 0.012% L-cysteine, and 0.016% L-methionine) containing 0.1% glucose and 1 M sorbitol to an equal volume of the samples. After the pulse-chase, ice-cold sodium azide was added to spheroplast suspensions to a final concentration of 10 mM, and the suspensions were separated by centrifugation into spheroplasts and media as the intracellular and extracellular fractions, respectively. Both fractions were subjected to immunoprecipitation using rabbit anti-invertase antibodies.

To assay total proteins secreted into the medium, cells were grown to mid-logarithmic phase in MV-low sulfate medium containing 5% glucose at 37°C for 2 h. Three OD_{600} units of cells were collected, resuspended in MV-no sulfate medium containing 2% glucose and 0.03% bovine serum albumin, and grown at 37°C for 30 min. The cells were labeled with 100 μCi of Tran^{35}S-label per OD_{600} unit of cells at 37°C for 15 min. A chase was initiated by adding the chase solution containing 2% glucose and 0.5% casamino acids to an equal volume of the samples. After a 45-min chase, cell suspensions were treated with sodium azide and separated into intracellular and extracellular fractions as described above. Trichloroacetic acid (TCA) was added to both fractions to a final concentration of 10%, and the fractions were kept on ice for 15 min, followed by centrifugation at 20,630 $\times$ *g* for 15 min. After one wash with 10% TCA and two washes with ice-cold acetone, pellets were solubilized in SDS-PAGE sample buffer.

To examine the sorting pathway for CPY, cells were pulse chased as described above. After a chase, cells were suspended in spheroplast stop solution (1 M sorbitol, 25 mM Tris-HCl, pH 7.5, 20 mM NaN_3, 10 mM dithiothreitol, and 20 mM NaF) and treated with 2.5 U/ml Zymolyase 100T. Intracellular and extracellular fractions were prepared as in the assay for invertase and subjected to immunoprecipitation by using rabbit anti-CPY antibodies.

RESULTS

Cdc50 Family Proteins Form Complexes with Drs2 Family Proteins

In a previous study, we demonstrated that Cdc50p and Lem3p associate with Drs2p and Dnf1p, respectively (Saito *et al.*, 2004). Dnf1p and its close homologue Dnf2p (83% similar and 69% identical at the amino acid sequence level) exhibit redundant activities in phospholipid translocation across the plasma membrane (Pomorski *et al.*, 2003; our unpublished data). Therefore, we examined whether Lem3p physically associates with Dnf2p in coimmunoprecipitation experiments. We constructed a gene that encoded a C-terminally Myc-tagged version of Dnf2p and introduced it into cells. Dnf2p-Myc was immunoprecipitated with an anti-Myc antibody from membrane protein extracts prepared by solubilization in 1% CHAPS. Lem3p was coimmunoprecipitated with Dnf2p-Myc, whereas Lem3p was not detected in immunoprecipitates from cells lacking *DNF2-Myc* (Figure 1A). In addition, Dnf2p-EGFP as well as Dnf1p-EGFP was localized in the ER in the *lem3*Δ mutant (Figure 1B). Neither Cdc50p nor Crf1p-HA was coimmunoprecipitated with Dnf2p-Myc, and Dnf2p-EGFP was localized to the plasma membrane in *cdc50*Δ and *crf1*Δ mutants (our unpublished data). Both Crf1p and Dnf3p colocalize with markers for early/late endosomes or the TGN, and deletion of either

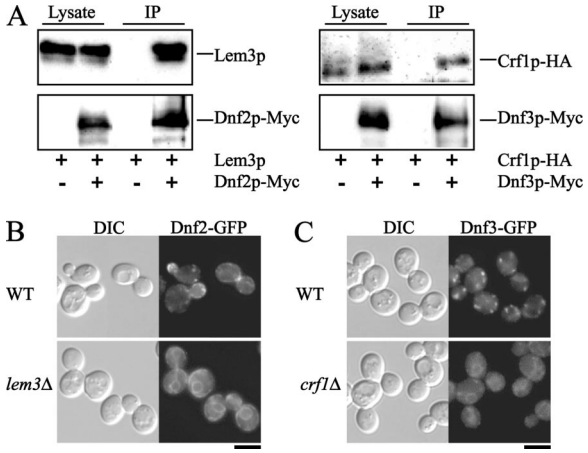

Figure 1. Cdc50 family proteins form complexes with Drs2 family proteins. (A) Coimmunoprecipitation of Lem3p and Crf1p with Dnf2p and Dnf3p, respectively. Cells were grown at 25°C to a cell density of 0.5 OD_{600}/ml in YPDA medium. Membrane extracts were then prepared as described in *Materials and Methods*. Myc-tagged Dnf2p or Dnf3p was immunoprecipitated with an anti-Myc antibody from these extracts. Immunoprecipitates were subjected to SDS-PAGE, followed by immunoblot analysis using antibodies against Lem3p or HA (top) and Myc (bottom). The results shown are representative of several experiments. The strains used were as follows: YKT1099 (*DNF2-Myc LEM3*) and YKT1098 (*DNF2 LEM3*) (left) and YKT1100 (*DNF3-Myc CRF1-HA*) and YKT1098 (*DNF3 CRF1-HA*) (right). (B) Localization of Dnf2p-EGFP. Wild-type (YKT921) and *lem3*Δ (YKT923) cells containing the *DNF2-EGFP* construct in the genome were grown to early to mid-logarithmic phase in YPDA medium at 30°C and immediately observed by fluorescence microscopy. (C) Localization of Dnf3p-EGFP. Wild-type (YKT925) and *crf1*Δ (YKT928) cells containing the *DNF3-EGFP* construct in the genome were grown and observed as described in (B). Bars, 5 μm.

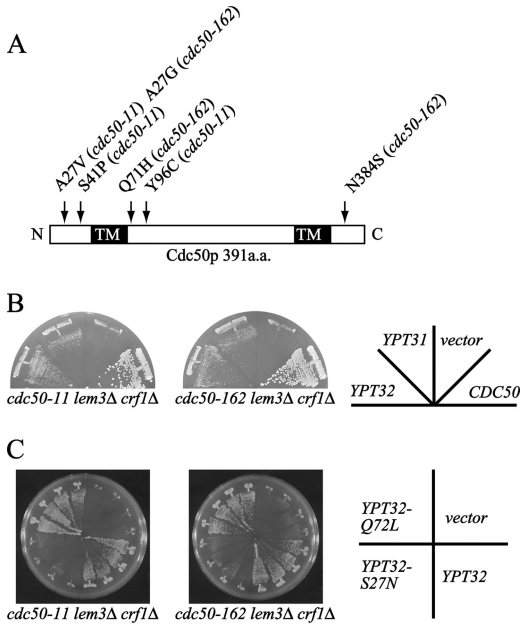

Figure 2. Overexpression of *YPT32* or *YPT31* suppresses the temperature-sensitive growth defect of the *cdc50-ts* mutants. (A) The domain structure of Cdc50p and the amino acid substitutions in Cdc50-11p and Cdc50-162p. The black boxes indicate potential transmembrane domains. (B) Suppression of the *cdc50-ts* mutations by multicopy *YPT32* or *YPT31*. *cdc50-11* (YKT993) and *cdc50-162* (YKT942) cells were transformed with pKT1555 (YEplac181-*YPT32*), pKT1554 (YEplac181-*YPT31*), pKT1259 (YEplac181-*CDC50*), or a control vector (YEplac181). Transformants were streaked onto a YPDA plate, followed by incubation at 37°C for 2 d. (C) The GTP-bound form, but not the GDP-bound form, of Ypt32p suppresses the ts growth defect of *cdc50-ts* mutants. *cdc50-11* (YKT993) and *cdc50-162* (YKT942) mutant cells were transformed with pKT1578 (YEplac181-$YPT32^{Q72L}$), pKT1579 (YEplac181-$YPT32^{S27N}$), pKT1555 (YEplac181-*YPT32*), or a control vector (YEplac181). For each plasmid, four independent transformants were streaked onto a YPDA plate, followed by incubation at 37°C for 3 d.

CRF1 or *DNF3* resulted in no discernible phenotypes (Hua *et al.*, 2002; Pomorski *et al.*, 2003; our unpublished observation). We examined whether Crf1p binds to Dnf3p in coimmunoprecipitation experiments. We created cells expressing both a C-terminally Myc-tagged version of *DNF3* and an HA-tagged version of *CRF1*. Crf1p-HA was coimmunoprecipitated with Dnf3p-Myc, whereas Crf1p-HA was not detected in immunoprecipitates from cells lacking *DNF3-Myc* (Figure 1A). In addition, Dnf3p-EGFP was localized in the ER of the *crf1*Δ mutant (Figure 1C). Neither Cdc50p nor Lem3p was coimmunoprecipitated with Dnf3p-Myc, and the localization patterns of Dnf3p-EGFP in *cdc50*Δ and *lem3*Δ mutants were identical to that in wild-type cells (our unpublished data). In addition, neither Drs2p-Myc nor Dnf1p-Myc coimmunoprecipitated with Crf1p-HA, and the localization patterns of Drs2p-EGFP and Dnf1p-EGFP in the *crf1*Δ mutant were identical to that in wild-type cells (our unpublished data). These results, together with our previous study (Saito *et al.*, 2004), demonstrate that Cdc50 family proteins (Cdc50p, Lem3p, and Crf1p) form complexes with Drs2 family proteins (Drs2p, Dnf1p and Dnf2p, and Dnf3p, respectively) in vivo.

Isolation of YPT32 as a Multicopy Suppressor of a cdc50-ts Mutation

To facilitate studies of the essential functions of putative PLTs composed of members of the Cdc50p and Drs2p families except for Neo1p, we constructed ts mutants of *CDC50* in the *lem3*Δ *crf1*Δ background (hereafter referred to as the *cdc50-ts* mutants). We obtained two mutants, *cdc50-11 lem3*Δ *crf1*Δ and *cdc50-162 lem3*Δ *crf1*Δ (hereafter referred to as the *cdc50-11* and *cdc50-162* mutants, respectively), that grew well at 25°C, but exhibited a tight ts growth defect at 37°C. DNA sequencing of the two mutant alleles revealed that each allele contained three mutations that resulted in amino acid substitutions (A27V, S41P, and Y96C in *cdc50-11* and A27G, Q71H, and N384S in *cdc50-162*) (Figure 2A). All substitution sites except for N384S were located in the N-terminal quarter of the protein. The alanine residue at position 27, a residue that was mutated in both alleles, is conserved among Cdc50p homologues in *Caenorhabditis elegans*, *Drosophila melanogaster*, and *Homo sapiens*.

We examined the growth profiles of the *cdc50-ts* mutants after a shift to 37°C. We counted the number of cells at 1, 2, 3, and 4 h after the shift and found that *cdc50-ts* mutants rapidly stopped growing at 37°C (Supplemental Figure S1A). Because Drs2p-EGFP was localized in the ER in the *cdc50*Δ mutant (Saito *et al.*, 2004), we next examined the localization of Drs2p-EGFP in the *cdc50-11* mutant after the shift to 37°C. At 25°C (0 min), Drs2p-EGFP was observed in punctate structures scattered throughout the cell and partially localized to the ER, although the fluorescence of Drs2p-EGFP was much less clear in the *cdc50-11* mutant than in wild-type cells (Supplemental Figure S1B). When incubated at 37°C for 1 h, there was a substantial decrease of

Drs2p-EGFP observed in punctate structures and in the ER in the *cdc50-11* mutant. After a 2-h incubation at 37°C, fluorescence of Drs2p-EGFP was barely detectable, although the very faint fluorescence was localized to the ER and a few large compartments located in the bud or near the bud neck (Supplemental Figure S1B). These results suggested that the Cdc50p–Drs2p complex was rapidly inactivated or degraded at 37°C. We analyzed phenotypes of the *cdc50-ts* mutants after 2- to 3-h incubation at 37°C in further experiments.

To obtain clues to essential functions of the *CDC50* and *DRS2* families, we screened for multicopy suppressors of the growth defect of the *cdc50-ts* mutants at 37°C. We found that overexpression of *YPT32* suppressed, albeit weakly, the growth defect of the *cdc50-ts* mutants (Figure 2B). Ypt32p, a Rab family small GTPase, shares a high degree of sequence similarity (81% identity and 90% similarity) with Ypt31p, overproduction of which also weakly suppressed the growth defect of the *cdc50-ts* mutants (Figure 2B). Overexpression of $YPT32^{Q72L}$, which mimics a GTP-bound form of the protein, but not of $YPT32^{S27N}$, which mimics a GDP-bound form, suppressed the ts growth phenotype of the *cdc50-ts* mutants to the same extent as overexpression of *YPT32* (Figure 2C), suggesting that *YPT32* suppressed the *cdc50-ts* mutations by hyperactivation of its downstream pathway through its effectors. Previous studies have reported that *YPT31/32* are involved in intra-Golgi transport, the formation of transport vesicles at the TGN (Benli *et al*., 1996; Jedd *et al*., 1997), and the recruitment of Sec2p, the guanine nucleotide exchange factor for Sec4p, to secretory vesicles (Ortiz *et al*., 2002). Therefore, we investigated the vesicular trafficking phenotypes in the *cdc50-ts* mutants.

The Secretory Pathway Seems Normal in a cdc50-ts Mutant

Because *YPT31/32* have been shown to be required for exit from the TGN in the exocytic pathway (Benli *et al*., 1996; Jedd *et al*., 1997) and the *drs2*Δ mutant exhibits defects in Golgi function (Chen *et al*., 1999; Hua *et al*., 2002), we investigated defects in the secretory pathways of the *cdc50-11* mutant. We first tested for the secretion of the periplasmic enzyme invertase. Because invertase acquires *N*-linked oligosaccharide chains, which are heterogeneously modified in the Golgi, it is secreted as a highly glycosylated protein and thus occurs as a high-molecular-mass smear after SDS-PAGE. In secretory mutants, invertase secretion is inhibited and the enzyme accumulates in the lumen of secretory compartments. Cells were incubated at 37°C for 2.5 h, induced to produce invertase for 30 min, pulse labeled for 7 min with Tran^{35}S-label, and chased at 37°C. After 15 min of chase, wild-type cells secreted most of the invertase as a fully glycosylated form. In the *cdc50-11* mutant, invertase was also secreted in a fully glycosylated form with kinetics similar to those of wild-type cells, whereas with a control secretory mutant, *sec2-56* (Novick *et al*., 1980), invertase remained intracellular even after a 30-min chase (Figure 3A). To examine a kinetic delay of invertase secretion more precisely, cells were pulse labeled for 2 min and chased for 2, 5, 10, and 15 min. In the *cdc50-11* mutant, invertase was secreted in a fully glycosylated form with kinetics similar to that of wild-type cells after a 10-min chase, although a slight delay was observed in the external appearance of invertase after a 5-min chase (Figure 3B).

To test whether the *cdc50-ts* mutants exhibited a cargo-specific defect in protein transport, we next examined general secretion in the *cdc50-11* mutant. Cells were incubated at 37°C for 2.5 h, pulse labeled with Tran^{35}S-label for 15 min, and chased for 45 min. Cells and media were separated by centrifugation into the intracellular and extracellular fractions, respectively. Judging from the band intensities in the intracellular fractions, the overall level of protein synthesis was similar among wild-type, *cdc50-11*, and *sec2-56* cells. In the extracellular fractions, wild-type and *cdc50-11* mutant cells exhibited similar levels of protein secretion into the medium, whereas the *sec2-56* mutant secreted almost no proteins (Figure 3C). These results suggest that secretion from the *cdc50-11* mutant was nearly normal.

Harsay and Bretscher (1995) used the ts late-acting *sec* mutant *sec6-4* to demonstrate that newly synthesized secretory proteins are exported via at least two different classes of secretory vesicles, which have similar diameters, but differ in their densities. The high-density vesicles (HDSVs) contain the soluble, secreted enzymes invertase and acid phosphatases together with most of the exoglucanase activity, whereas the low-density vesicles (LDSVs) contain the plasma membrane H^+-ATPase Pma1p (Harsay and Bretscher, 1995; David *et al*., 1998). Disruption of a gene encoding a dynamin-related protein (*VPS1*) or the clathrin heavy chain (*CHC1*) abolishes the production of HDSVs, yielding LDSVs that contain all the secreted cargo (Gurunathan *et al*., 2002). Because *DRS2* was implicated in the formation of clathrin-coated vesicles (Chen *et al*., 1999; Gall *et al*., 2002), we examined whether the production of these two types of secretory vesicles was affected in the *cdc50-11* mutant. We created a quadruple *cdc50-11 lem3*Δ *crf1*Δ *sec6-4* mutant (*cdc50-11 sec6-4* mutant) and purified secretory vesicles by Nycodenz density gradient centrifugation of membranes prepared from temperature-shifted *cdc50-11 sec6-4*, or *sec6-4* mutant cells. Western blots of the gradient fractions indicated that Pma1p levels were highest in the lower density membranes from the *cdc50-11 sec6-4* mutant as well as from the *sec6-4* mutant (Figure 3D), whereas the activities of invertase, acid phosphatase, and exoglucanase were found in the higher density fractions from both the *cdc50-11 sec6-4* and *sec6-4* mutants (Figure 3E). We also carried out the density gradient purification of membranes from *sec6-4* and *cdc50-11 sec6-4* cells grown at the permissive temperature (25°C). Pma1p was not detected by Western blots of any gradient fractions from *sec6-4* and *cdc50-11 sec6-4* cells (our unpublished data). Similarly, activities of invertase, acid phosphatase, and exoglucanase were not found in any fractions from both the *sec6-4* and *sec6-4 cdc50-11* mutants (our unpublished data). These results suggested that the activities of invertase, acid phosphatase, and exoglucanase and the Pma1p levels observed in the density gradient fractions from both strains incubated at 37°C reflected the high- and low-density classes of exocytic vesicles, respectively. These results suggest that the *cdc50-11* mutant did not exhibit major defects in production of these two types of secretory vesicles.

The Endocytic Pathway to the Vacuole and the Vacuolar Protein Sorting Pathway Seems Normal in the cdc50-ts Mutants

Endocytic transport from the plasma membrane to the vacuole was previously examined in *dnf* and *drs2* mutants. Defective endocytic internalization of the lipophilic dye FM4-64 and α-mating factor was demonstrated in the *dnf1*Δ *dnf2*Δ *drs2*Δ mutant (Pomorski *et al*., 2003), whereas the *drs2*Δ, *cdc50*Δ, and *dnf1*Δ *dnf2*Δ *dnf3*Δ mutants were shown to be defective in a certain step in the postinternalization transport to the vacuole (Chen *et al*., 1999; Hua *et al*., 2002; Misu *et al*., 2003). All these assays were conducted at lower temperatures such as 15 or 18°C. The *cdc50-ts* mutants, however, internalized and delivered FM4-64 to the vacuole at

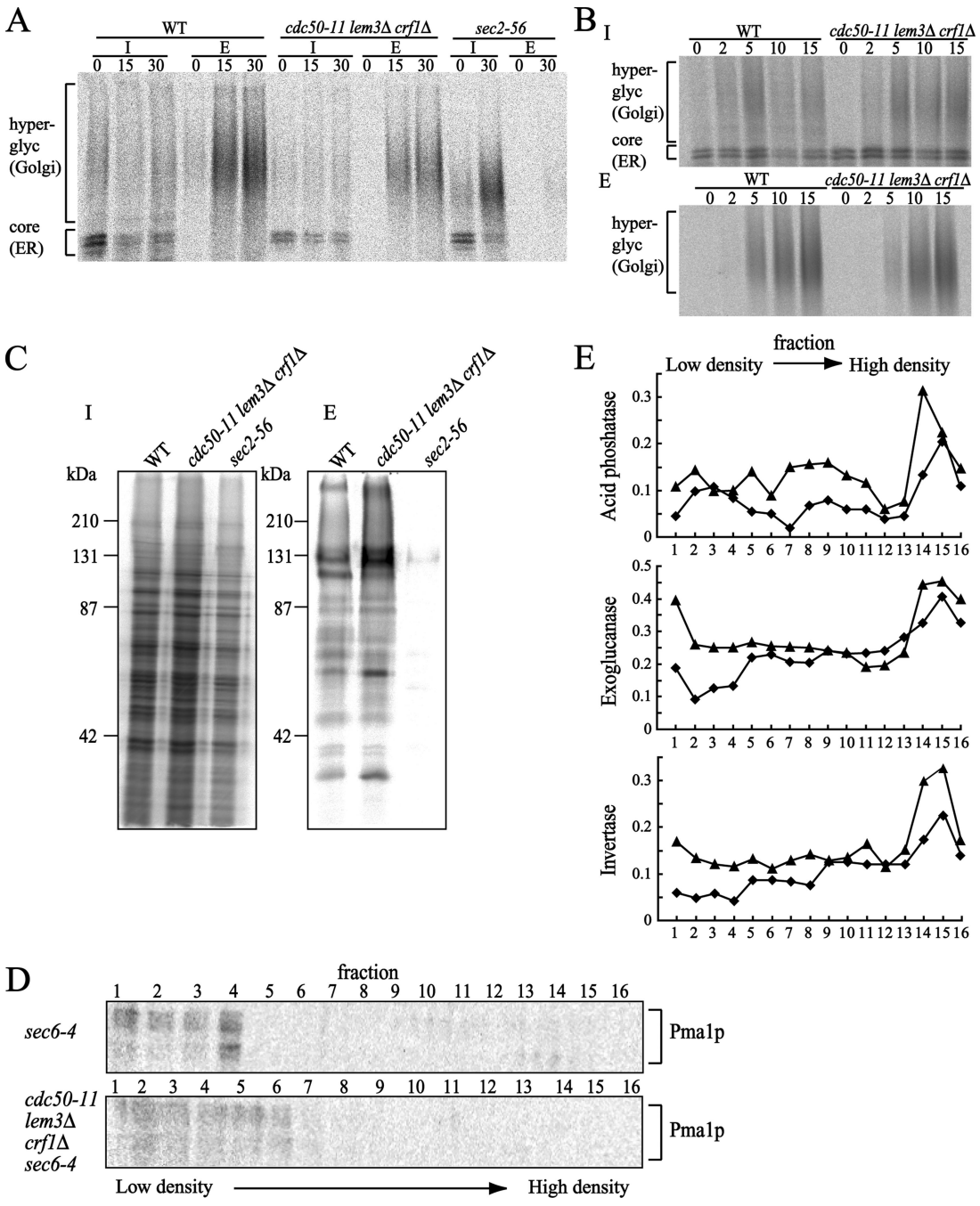

Figure 3. Secretion and formation of secretory vesicles are nearly normal in a *cdc50-ts* mutant. (A and B) Pulse-chase experiments of invertase secretion. Wild-type (YKT38), *cdc50-11* (YKT993), and *sec2-56* (ANS2-3A) cells (A) or wild-type (YKT38) and *cdc50-11* (YKT993) cells (B) were grown for 2.5 h at 37°C, induced to produce invertase for 30 min, pulse labeled with Tran^{35}S-label for 7 min (A) or 2 min (B), and chased for the indicated time at 37°C. Samples were separated by centrifugation into internal (I) and external (E) fractions. Invertase was recovered by immunoprecipitation and visualized by SDS-PAGE and a phosphorimager system. (C) General secretion by the *cdc50-11* mutant. Wild-type (YKT38), *cdc50-11* (YKT993), and *sec2-56* (ANS2-3A) cells were grown for 2.5 h at 37°C, pulse labeled with Tran^{35}S-label for 15 min, and chased for 45 min. Samples were separated by centrifugation into I and E fractions. Proteins in each fraction were precipitated with TCA and visualized by SDS-PAGE and a phosphorimager system. (D) Western blots for Pma1p, a marker for low-density vesicles, in Nycodenz gradient fractions. *sec6-4* (YKT1010) and *cdc50-11 sec6-4* (YKT1011) cells transformed with pKT1486 (P_{ACT1}-*SUC2*) were incubated for 2 h at 37°C. Secretory vesicles were prepared and fractionated as described in *Materials and Methods*. Numbered fractions (as indicated at the top) were heated in sample buffer for 15 min at 37°C, separated by SDS-PAGE, and probed with antibodies against Pma1p. (E) Activities of marker enzymes for high-density vesicles in Nycodenz gradient fractions. Fractions were prepared from *sec6-4* (diamonds) and *cdc50-11 sec6-4* (triangles) cells as described in D. Hydrolyzing enzyme activities are expressed in arbitrary units based on the absorbance measured at 415 nm (acid phosphatase, top; exoglucanase, middle) or at 540 nm (invertase, bottom).

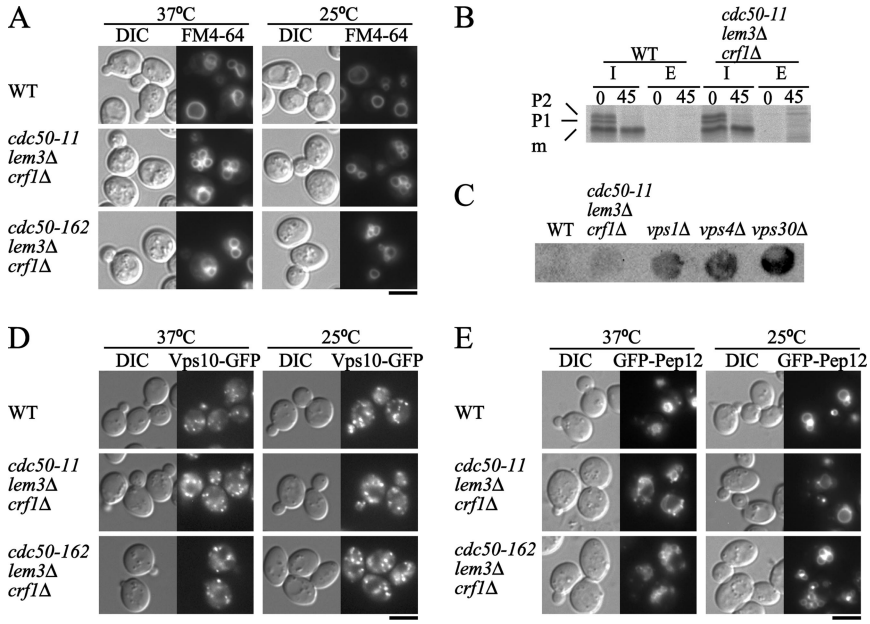

Figure 4. Normal endocytic and VPS pathways in the *cdc50-ts* mutants. (A) Internalization and transport of FM4-64 to the vacuole. Wild-type (YKT38), *cdc50-11* (YKT993), and *cdc50-162* (YKT942) cells grown for 3 h were stained with FM4-64 for 15 min in YPDA medium, and chased for 30 min in fresh YPDA medium, at the indicated temperature. Bar, 5 μm. (B) Pulse-chase experiments of CPY intracellular transport. Wild-type (YKT38) and *cdc50-11* (YKT993) cells were grown for 2.5 h at 37°C, pulse labeled with Tran^{35}S-label for 15 min, and chased for 45 min at 37°C. CPY was immunoprecipitated from I and E fractions, resolved by SDS-PAGE, and visualized using a phosphorimager system. (C) Secretion of CPY. Wild-type (YKT38), *cdc50-11* (YKT993), *vps1*Δ (KKT276), *vps4*Δ (KKT277), and *vps30*Δ (AKY15) cells were grown for 3 h at 37°C in contact with a nitrocellulose filter, and secreted CPY was detected by probing with antibodies against CPY. (D) Localization of Vps10p-EGFP. Wild-type (YKT957), *cdc50-11* (YKT1086), and *cdc50-162* (YKT1088) cells containing the *VPS10-EGFP* construct in the genome were grown for 3 h at 25 or 37°C in SD medium. Bar, 5 μm. (E) Localization of GFP-Pep12p. Wild-type (YKT38), *cdc50-11* (YKT993), and *cdc50-162* (YKT942) cells transformed with pKT1487 (pRS416-*GFP-PEP12*) were grown for 3 h at 25°C or 37°C in SDA-Ura medium. Bar, 5 μm.

37°C during a 30-min incubation (Figure 4A). Although the sizes of the vacuoles visualized by FM4-64 staining were somewhat smaller in the *cdc50-ts* mutants, this phenotype was not affected by the incubation temperature. These results suggest that the essential function of the putative PLTs at higher temperatures is not in endocytic transport from the plasma membrane to the vacuole.

Next, we assessed the vacuolar protein sorting (VPS) pathway by monitoring the maturation of a vacuolar soluble protein, CPY. Previous studies showed that *drs2*Δ, *cdc50*Δ, and *dnf1*Δ *drs2*Δ mutants exhibited a kinetic defect in CPY transport to the vacuole at lower temperatures (Chen *et al*., 1999; Hua *et al*., 2002; Misu *et al*., 2003). Wild-type and *cdc50-11* mutant cells were preincubated for 2.5 h, labeled with Tran^{35}S-label for 15 min, and chased for 45 min at 37°C. After a 15-min pulse, wild-type cells contained two precursor forms of CPY: a 67-kDa species (P1) in the ER and a fully glycosylated 69-kDa form (P2) in the Golgi. After a 45-min chase, precursors were cleaved to the 65-kDa mature form (m) after delivery to the vacuole by proteinase A (Stevens *et al*., 1982). Analysis of the *cdc50-11* mutant showed that transport from the ER to the Golgi and from the Golgi to the vacuole occurred at normal rates (Figure 4B). Some class E *vps* mutants are capable of forming mature CPY at nearly normal rates despite a defect in the VPS pathway, because vacuolar proteases are mature in the class E compartment. The class E *vps* mutants, however, secrete a significant fraction of CPY into the medium (Raymond *et al*., 1992), whereas the *cdc50-11* mutant did not secrete CPY into the extracellular space (Figure 4B). This result was confirmed by colony blot assays (Roberts *et al*., 1991; Wiederkehr *et al*., 2000), by which secreted CPY can be detected. In contrast to *vps1*Δ, *vps30*Δ (class A) and *vps4*Δ (class E), the *cdc50-11* mutant did not secrete significant amounts of CPY (Figure 4C). These results suggest that the VPS pathway is not affected in the *cdc50-11* mutant at higher temperatures.

The membrane-bound CPY-sorting receptor Vps10p has been reported to cycle between the TGN and late endosomes (Cereghino *et al*., 1995; Cooper and Stevens, 1996), and a complex called the "retromer," which comprises five proteins, is required for the endosome-to-TGN retrieval of Vps10p (Seaman *et al*., 1997). Thus, the removal of components of the retromer results in missorting of Vps10p to the vacuole (Seaman *et al*., 1997). We created cells expressing a C-terminally EGFP-tagged version of *VPS10* and observed the localization of Vps10p-EGFP. In wild-type cells, Vps10p-EGFP resulted in a punctate fluorescence pattern characteristic of TGN-localized yeast proteins (Figure 4D) as described previously (Cereghino *et al*., 1995; Cooper and Stevens, 1996). Similarly, Vps10p-EGFP created a punctate fluorescence pattern in the *cdc50-11* and *cdc50-162* mutants incubated at 37°C as well as 25°C (Figure 4D), suggesting that Vps10p-EGFP was normally retrieved from late endosomes in the *cdc50-ts* mutants. These results are consistent with our observation that CPY sorting was normal in the *cdc50-11* mutant (Figure 4, B and C).

We also analyzed the localization of the endosomal syntaxin Pep12p. Whereas endogenous Pep12p typically occurs as scattered or perivacuolar puncta (Lewis *et al*., 2000), GFP-Pep12p, the expression of which was driven by the strong *TPI1* promoter, reached the vacuolar outer membrane via late endosomes (Black and Pelham, 2000). We observed the localization of GFP-Pep12p expressed under the control of the *TPI1* promoter in the *cdc50-ts* mutants. In wild-type cells and the *cdc50-ts* mutants, GFP-Pep12p was found in small punctate structures and vacuolar membranes at 25 and 37°C (Figure 4E). The small punctate structures seemed to be late endosomes, because they were much smaller than the vacuoles. These results suggest that in the *cdc50-ts* mutants, GFP-Pep12p was normally transported to late endosomes, and overexpressed GFP-Pep12p was further delivered to the vacuole.

Together, our results suggest that the *cdc50-ts* mutants do not have major defects in the endocytic pathway to the vacuole, the VPS pathway, or the recycling pathway between the TGN and late endosomes. Thus, PLTs composed of proteins from the Cdc50p and Drs2p families are unlikely to be essential for membrane trafficking via these pathways at higher temperatures.

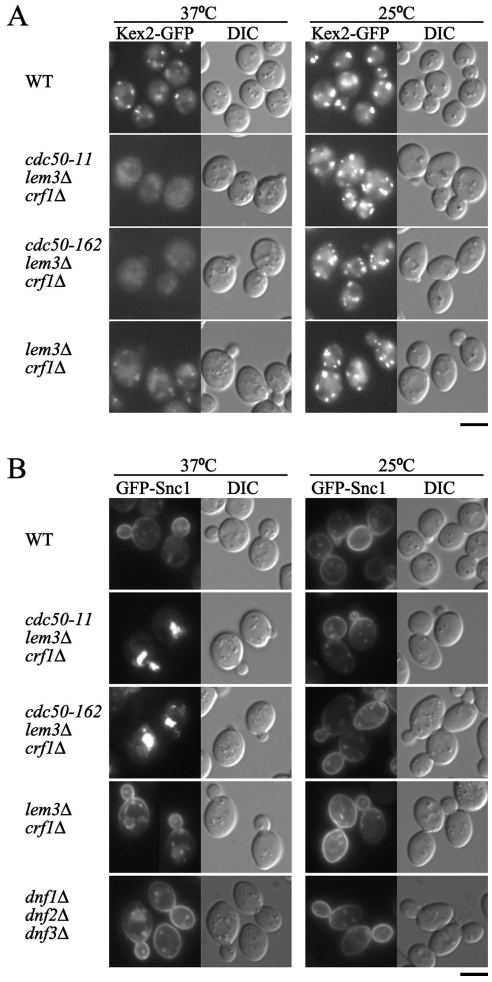

Figure 5. Recycling marker proteins are mislocalized in the *cdc50-ts* mutants. (A) Localization of Kex2p-EGFP. Wild-type (YKT903), *cdc50-11* (YKT1000), *cdc50-162* (YKT1001), and *lem3*Δ *crf1*Δ (YKT1310) cells containing the *KEX2-EGFP* construct in the genome were grown for 3 h at 25 or 37°C in SD medium. (B) Localization of GFP-Snc1p. Wild-type (YNF63), *cdc50-11* (YNF65), *cdc50-162* (YNF67), *lem3*Δ *crf1*Δ (YNF61), and *dnf1*Δ *dnf2*Δ *dnf3*Δ (YNF784) cells carrying the pRS416-*GFP-SNC1* plasmid were grown for 3 h at 25 or 37°C in SDA-Ura medium. Bars, 5 μm.

cdc50-ts Mutants Show Mislocalization of Recycling Proteins

During the course of this study, Segev and colleagues reported that Ypt31p/32p are also involved in the retrieval of the furin homologue Kex2p and the v-SNARE Snc1p from endosomes to the TGN (Chen *et al*., 2005). Thus, we examined localization of GFP-tagged versions of these proteins in the *cdc50-ts* mutants. Kex2p is a TGN resident protein that is localized due to constant retrieval from late and early endosomes (Brickner and Fuller, 1997; Lewis *et al*., 2000). At 25°C, C-terminally EGFP-tagged Kex2p resulted in cytoplasmic fluorescent puncta typical of proteins that are localized in the yeast TGN (Figure 5A). We also observed weak fluorescent signals that seem to correspond to vacuoles as judged by colocalization with CellTracker Blue CMAC, a dye that stains the vacuolar lumen (Supplemental Figure S2). In *lem3*Δ *crf1*Δ mutant cells incubated at 37°C, punctate localization patterns of Kex2p-GFP were observed as in wild-type cells, although they were less clear. In contrast, in the *cdc50-ts* mutants incubated at 37°C, Kex2p-EGFP was primarily localized in vacuoles (Figure 5A and Supplemental Figure S2), as was demonstrated in the *ypt31*Δ *ypt32-ts* mutant (Chen *et al*., 2005). Similar to Vps10p, Kex2p mislocalizes to the vacuole when cycling between endosomes and the TGN is impaired (Wilcox *et al*., 1992; Cooper and Stevens, 1996; Conibear and Stevens, 2000). Because Vps10p exhibited the normal punctate localization in the *cdc50-ts* mutants (Figure 4D), our results suggest that the *cdc50-ts* mutants are defective in the retrieval pathway from early endosomes.

Snc1p is recycled from the plasma membrane via early endosomes to the TGN (Lewis *et al*., 2000). Previous studies reported that Snc1p was mislocalized in the *cdc50*Δ, *drs2*Δ, and *dnf1*Δ *dnf2*Δ *dnf3*Δ mutants (Hua *et al*., 2002; Saito *et al*., 2004). In wild-type, *lem3*Δ *crf1*Δ, and *cdc50-ts* mutant cells at 25°C, GFP-Snc1p was primarily localized to the plasma membrane at a polarized site, such as a growing bud or a cytokinesis site, with a small fraction of GFP-Snc1p observed in intracellular punctate structures (Figure 5B). In the *lem3*Δ *crf1*Δ mutants at 37°C, GFP-Snc1p was also localized to the plasma membrane at a polarized site, although GFP-Snc1p in internal structures slightly increased (Figure 5B). In contrast, in the *cdc50-ts* mutants at 37°C, GFP-Snc1p accumulated in a few large compartments located in the bud or near the bud neck, with a concomitant decrease in the amount of the protein observed at the plasma membrane (Figure 5B). These results suggested that the *lem3*Δ *crf1*Δ double mutations did not cause the mislocalization of GFP-Snc1p but the combination of the inactivation of Cdc50p and the double mutations did. We also examined the localization of GFP-Snc1p in the *dnf1*Δ *dnf2*Δ *dnf3*Δ mutant. The localization pattern of GFP-Snc1p in the *dnf1*Δ *dnf2*Δ *dnf3*Δ mutant was very similar to that in the *lem3*Δ *crf1*Δ mutant both at 25 and 37°C (Figure 5B). This result is consistent with our conclusion that Lem3p and Crf1p interact with Dnf1p/2p and Dnf3p, respectively, and that the *lem3*Δ *crf1*Δ double mutations inactivate the Dnf1p, Dnf2p, and Dnf3p activity. However, our result that the *dnf1*Δ *dnf2*Δ *dnf3*Δ mutant did not exhibit a major defect for the localization of GFP-Snc1p is inconsistent with a previous report by Hua *et al*. (2002), which showed that a substantial fraction of GFP-Snc1p was intracellularly localized. This contradiction may be due to differences of the strain background.

The atypical labeling of intracellular structures with GFP-Snc1p in the *cdc50-ts* mutants could result from defects in the transport pathway from the TGN to the plasma membrane or in that from the plasma membrane to the TGN via endosomes. When *cdc50-11* cells preincubated at 37°C for 3 h were treated with 100 μM of the actin assembly inhibitor latrunculin A (LAT-A) for 10 min at 37°C to block endocytosis, GFP-Snc1p was observed to be localized to the plasma membrane in addition to intracellular large structures (Figure 6A); the percentages of *cdc50-11* cells with GFP-Snc1p at the plasma membrane increased from 42% (n = 183) (dimethyl sulfoxide [DMSO] control) to 83% (n = 133) (LAT-A treatment). These results suggested that newly synthesized GFP-Snc1p reached the plasma membrane in the mutant cells. Consistent with this result, a mutant form of GFP-Snc1p, GFP-Snc1p-pm, which can reach the plasma membrane but cannot be internalized by endocytosis (Lewis *et al*., 2000), was exclusively localized to the plasma membrane in the *cdc50-11* mutant as well as wild-type cells at 37°C (Figure 6B). These results also suggest that GFP-Snc1p needs to be endocytosed to be incorporated into the large intracellular structures. To confirm this with GFP-fused wild-type Snc1p, cells grown at 25°C were pretreated with 100 μM LAT-A for

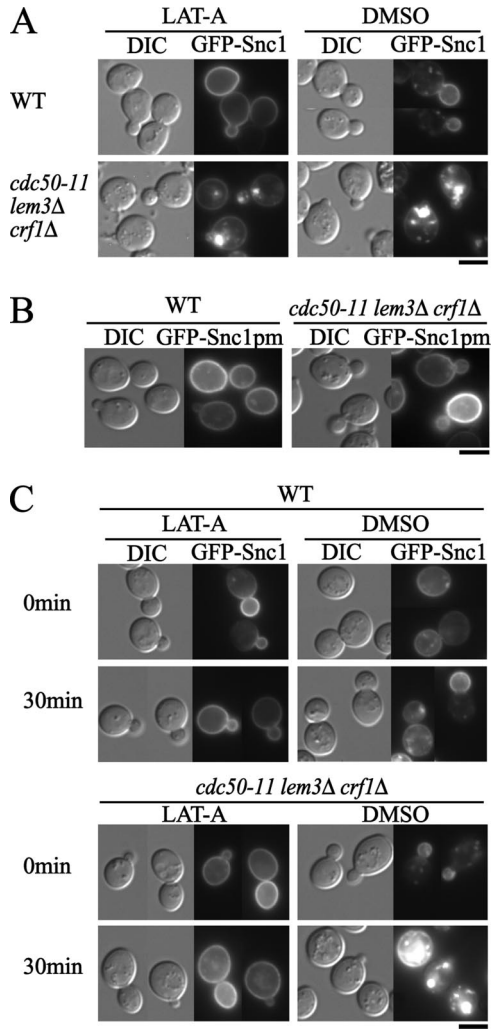

Figure 6. The *cdc50-ts* mutant is defective in plasma membrane-to-TGN transport. (A) Plasma membrane localization of GFP-Snc1p is restored in the *cdc50-ts* mutant by blocking endocytosis with LAT-A. Wild-type (YNF63) and *cdc50-11* (YNF65) cells carrying the pRS416-*GFP-SNC1* plasmid were preincubated at 37°C for 3 h and then treated with 100 μM LAT-A or DMSO (vehicle control) for 10 min at 37°C in SDA-Ura medium. (B) Localization of GFP-Snc1p-pm. Wild-type (YKT38) and *cdc50-11* (YKT993) cells transformed with pRS416-*GFP-SNC1 pm* were grown to early logarithmic phase at 25°C and shifted to 37°C for 3 h in SDA-Ura medium. (C) Pretreatment with LAT-A inhibits abnormal accumulation of GFP-Snc1p in the *cdc50-ts* mutant. Wild-type (YNF63) and *cdc50-11* (YNF65) cells carrying the pRS416-*GFP-SNC1* plasmid were grown to early logarithmic phase at 25°C and were then pretreated with 100 μM LAT-A or DMSO (vehicle control) for 10 min at 25°C in SDA-Ura medium (0 min), followed by incubation at 37°C for 30 min in SDA-Ura medium in the presence (LAT-A) or absence (DMSO) of 100 μM LAT-A (30 min). Bars, 5 μm.

10 min at 25°C (0 min), followed by incubation at 37°C for 30 min in the presence of 100 μM LAT-A (30 min) (Figure 6C). LAT-A treatment inhibited the intracellular accumulation of GFP-Snc1p in the *cdc50-11* mutant. These results suggest that *cdc50-11* mutant cells are defective in the plasma membrane-to-TGN transport pathway but not in the TGN-to-plasma membrane transport pathway.

Together, our results implicate putative PLTs in the retrieval pathway from early endosomes to the TGN. Ypt31p/32p and putative PLTs may functionally interact in this pathway.

Given that Snc1p accumulates in intracellular compartments in *ypt31Δ ypt32-ts* mutant cells (Chen *et al*., 2005), we tested for the effects of overproduction of the GTP-bound (Q72L) or GDP-bound (S27N) form of Ypt32p (Figure 2C) on the localization of GFP-Snc1p. In cells overexpressing $YPT32^{Q72L}$, GFP-Snc1p was primarily localized to the plasma membrane of the growing site as it was in wild-type cells. In contrast, GFP-Snc1p accumulated in abnormal compartments located in the bud or near the bud neck in ~15% of the cells carrying $YPT32^{S27N}$ (n = 149) (Supplemental Figure S3), similar to the results observed with the *cdc50-ts* mutants. Because Ypt31p/32p were implicated in transport out of the TGN (Benli *et al*., 1996; Jedd *et al*., 1997), we examined whether GFP-Snc1p-pm reached the plasma membrane in the mutant strains. GFP-Snc1p-pm was exclusively localized to the plasma membrane in cells carrying $YPT32^{S27N}$ or $YPT32^{Q72L}$ (Supplemental Figure S3). These results also suggest that *YPT32* is involved in endocytic recycling.

We next examined whether overexpression of *YPT32* suppressed mislocalization of GFP-Snc1p in the *cdc50-ts* mutants. When *YPT32* was overexpressed at 37°C, the percentages of *cdc50-11* and *cdc50-162* mutant cells with GFP-Snc1p at sites with polarized plasma membranes increased from 39% (n = 117) to 60% (n = 120) and from 43% (n = 170) to 55% (n = 141), respectively (our unpublished data). Similarly, the percentages of *cdc50-11* and c*dc50-162* mutant cells with GFP-Snc1p in large compartments at 37°C slightly decreased from 44% (n = 119) to 35% (n = 132) and from 38% (n = 120) to 28% (n = 140), respectively (our unpublished data). These results are consistent with a weak suppression of the growth defect in the *cdc50-ts* mutants by overexpression of *YPT32* (Figure 2B). In addition, overexpression of *YPT32* did not suppress the cold-sensitive growth phenotype of the *cdc50Δ* mutant at 18°C (our unpublished data). These results suggest that *YPT32* is not a bypass suppressor of the *cdc50* mutations and thus raise the possibility that *YPT32* requires the residual PLT activity of Cdc50p-Drs2p for the suppression.

In the cdc50-11 Mutant, GFP-Snc1p and GFP-Tlg1p Seem to Accumulate in Early Endosome-derived Structures

We morphologically examined the Snc1p-containing structures in the *cdc50-11* mutant. To examine whether the large structures were associated with the TGN, the TGN was visualized with a TGN marker, C-terminally mRFP1-tagged Sec7p (Franzusoff *et al*., 1991), in *cdc50-11* mutant cells expressing *GFP-SNC1*. Although Sec7p-mRFP1 was observed in punctate structures scattered throughout wild-type and *cdc50-11* mutant cells at 37°C, few of the GFP-Snc1p–positive structures were colocalized with Sec7p-mRFP1 (Figure 7A), suggesting that the large GFP-Snc1p-labeled structures were not associated with the TGN. We next examined whether a recycling defect in the *cdc50-ts* mutants caused GFP-Snc1p to be missorted to the vacuole as with Kex2p-EGFP. Few of the GFP-Snc1p–positive structures, however, were also stained by CellTracker Blue CMAC (Figure 7B), suggesting that GFP-Snc1p did not accumulate in the vacuole. Thus, our results suggest that GFP-Snc1p is associated with endosomal structures.

RCY1 is involved in endocytosis and recycling out of early endosomes (Wiederkehr *et al*., 2000). Chen *et al*. (2005) have proposed that Rcy1p functions as an effector of Ypt31p/32p and that in the *ypt31Δ ypt32-ts* mutant, GFP-Snc1p is mostly localized to intracellular compartments as in *RCY1* null mu-

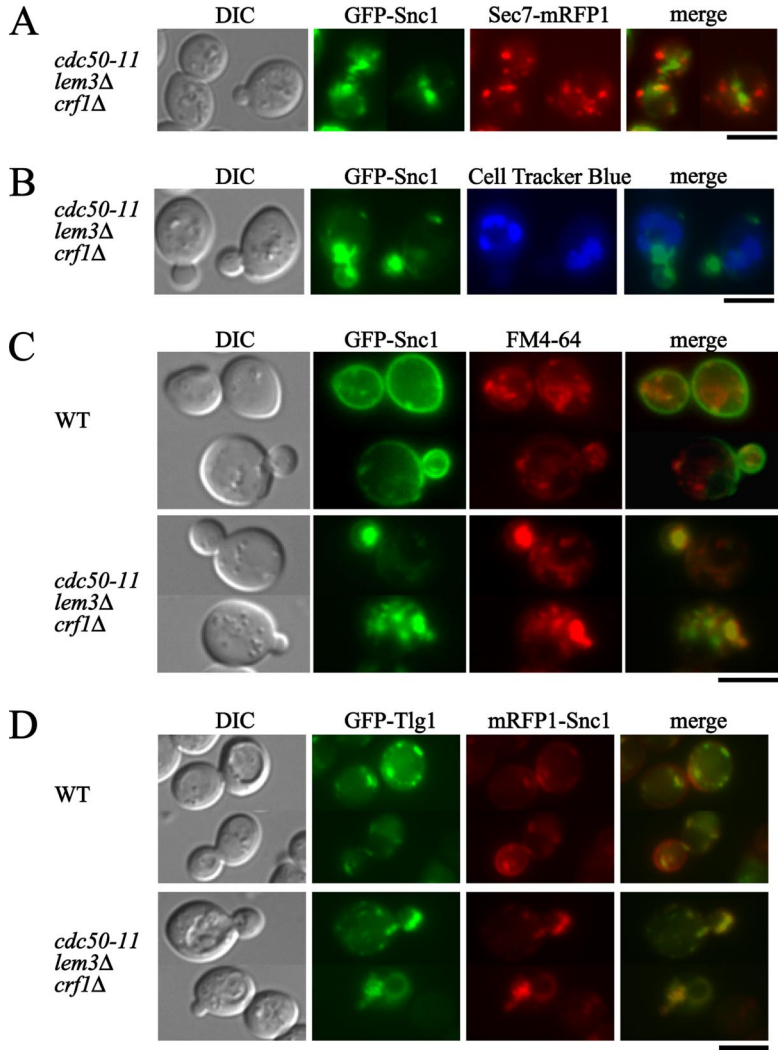

Figure 7. GFP-Snc1p and GFP-Tlg1p accumulate in early endosome-derived structures in the *cdc50-ts* mutant. (A) GFP-Snc1p and the TGN marker Sec7p-mRFP1 are not colocalized in the *cdc50-11* mutant. *cdc50-11 SEC7-mRFP1* (YNF153) cells carrying pRS416-*GFP-SNC1* were incubated at 37°C for 3 h in SDA-Ura medium. Obtained images were merged to compare the two signal patterns. (B) GFP-Snc1p is not localized to vacuoles stained with CellTracker Blue CMAC in the *cdc50-11* mutant. *cdc50-11* (YNF65) cells carrying the pRS416-*GFP-SNC1* plasmid were grown at 37°C for 3 h, followed by staining with 100 μM CellTracker Blue CMAC at 37°C for 15 min. (C) GFP-Snc1p was colocalized with FM4-64 after a short incubation in the *cdc50-11* mutant. Wild-type (YNF63) and *cdc50-11* (YNF65) cells carrying the pRS416-*GFP-SNC1* plasmid were grown at 37°C for 3 h, stained with 32 μM FM4-64 on ice for 30 min, and chased in fresh medium at 37°C for 10 min. (D) mRFP1-Snc1p and GFP-Tlg1p are colocalized in the *cdc50-11* mutant. Wild-type (YKT38) and *cdc50-11* (YKT993) cells cotransformed with pKT1566 (YEplac181-*GFP-TLG1*) and pKT1563 (pRS416-*mRFP1-SNC1*) were incubated at 37°C for 3 h in SD-Leu-Ura medium, followed by microscopic examination after fixation with 0.5% formaldehyde. Bars, 5 μm.

tants. In both cases, the GFP-Snc1p–labeled abnormal compartments were suggested to be derived from early endosomes. Because the large GFP-Snc1p–labeled structures in the *cdc50-ts* mutants were reminiscent of those in the *rcy1*Δ mutants reported by Wiederkehr *et al.* (2000), we examined whether GFP-Snc1p is localized to early endosomes in the *cdc50-ts* mutants. To identify early endosomes, we used FM4-64, which stains early endosomes after short incubation (Vida and Emr, 1995). Cells were incubated at 37°C for 3 h, labeled with FM4-64 on ice for 30 min, and chased at 37°C for 10 min. In wild-type cells, 71% of FM4-64–positive punctate structures were colocalized with GFP-Snc1p-positive structures (n = 183), whereas 84% of GFP–Snc1p structures were colocalized with FM4-64 labeling (n = 183) (Figure 7C). These results suggest that most of the GFP-Snc1p–positive structures correspond to early endosomes, consistent with a previous report in which internal GFP-Snc1p–positive punctate structures were shown to be early endosomes or the TGN (Lewis *et al.*, 2000). In contrast, in *cdc50-11* mutant cells, FM4-64 was observed to label abnormally large structures, and 73% of these FM4-64–positive structures were colocalized with the large GFP-Snc1p–positive structures (n = 191; Figure 7C). Conversely, 90% of the large GFP-Snc1p–positive structures were colocalized with FM4-64–positive structures (n = 182; Figure 7C). These results suggest that GFP-Snc1p accumulated in the abnormal early endosome-derived structures in the *cdc50-11* mutant, as was observed in the *ypt31*Δ *ypt32-ts* and *rcy1*Δ mutants.

Because in the *rcy1*Δ mutant, the target membrane-associated (t)-SNARE Tlg1p seems to intracellularly accumulate in abnormal compartments (Wiederkehr *et al.*, 2000) as was observed for Snc1p, we examined the localization of Tlg1p in *cdc50-11* mutant cells. Tlg1p is recycled between the TGN and early endosomal membrane, and is consequently present in both membranes (Lewis *et al.*, 2000). To examine the localization of Tlg1p in the *cdc50-11* mutant, we constructed a multicopy plasmid containing *GFP-TLG1* driven by its own promoter. In wild-type cells, GFP-Tlg1p was observed to be scattered throughout the cell (Figure 7D). In contrast, there was a substantial decrease of GFP-Tlg1p localized to punctate structures in *cdc50-11* mutant cells, and GFP-Tlg1p was instead localized to large compartments (Figure 7D). To examine whether Tlg1p and Snc1p were localized in the same large compartments in *cdc50-11* mutant cells, we constructed a single-copy plasmid containing the *mRFP1-SNC1* gene driven by the *TPI1* promoter and examined cells coexpressing *GFP-TLG1* and *mRFP1-SNC1*. Quantitative analysis of individual spots revealed that in the *cdc50-11* mutant cells, 96% of the mRFP1-Snc1p–positive large structures were also labeled with GFP-Tlg1p (n = 170),

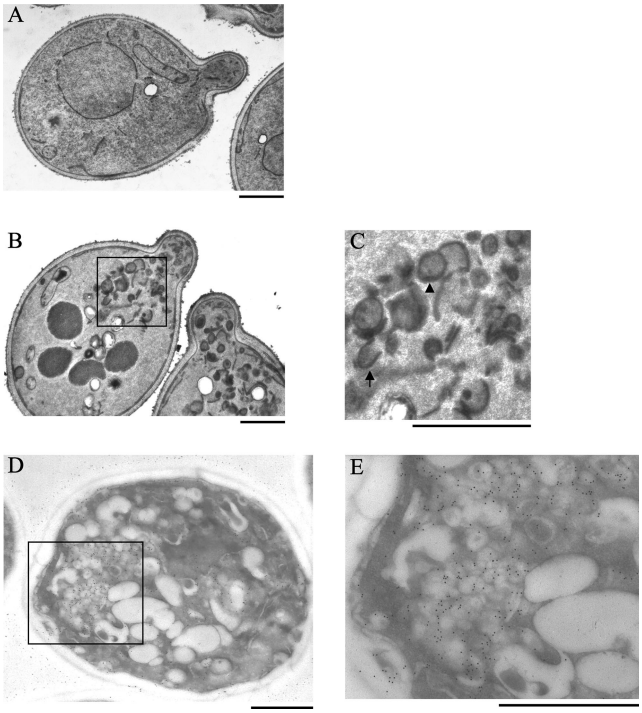

Figure 8. Electron microscopic examination of the abnormal structures containing HA-Snc1p in the *cdc50-ts* mutant. (A–C) The electron microscopic observation was performed using the glutaraldehyde-permanganate fixation technique. Wild-type (YKT38; A) and *cdc50-11* mutant cells (YKT993; B and C) were grown at 25°C to early logarithmic phase, shifted to 37°C, and grown in YPDA medium for 3 h. Cells were prepared for EM as described in *Materials and Methods*. The boxed region in B is enlarged in C. An arrow and an arrowhead indicate a horseshoe-like structure and a double-membrane ring, respectively. Bars, 1 μm. (D and E) Immunoelectron microscopic observation of the *cdc50-11* mutant was performed by the aldehyde fixation/metaperiodate permeabilization method. *cdc50-11* mutant cells (YKT993) transformed with pKT1564 (pRS416-*HA-SNC1*) were grown at 25°C to early logarithmic phase, shifted to 37°C, and grown in SDA-Ura medium for 3 h. Cells were prepared for immuno-EM as described in *Materials and Methods* and labeled with an anti-HA antibody. The boxed region in D is enlarged in E. Bars, 1 μm.

whereas 86% of the GFP-Tlg1–positive structures were also labeled with mRFP1-Snc1p (n = 163) (Figure 7D). These results suggest that the *cdc50-11* mutant was defective in the retrieval pathway from early endosomes to the TGN and that Snc1p and Tlg1p accumulated in the abnormal structures derived from early endosomes in the *cdc50-ts* mutants.

Electron Microscopic Examination of the Abnormal Structures Containing HA-Snc1p *in the cdc50-11 Mutant*

EM was performed to visualize and characterize the abnormally large compartments containing GFP-Snc1p in the *cdc50-ts* mutants by the glutaraldehyde-permanganate fixation technique. We found that these large structures were actually composed of a cluster of abnormal membranous structures. As shown in Figure 8, B and C, *cdc50-11* mutant cells incubated at 37°C accumulated a number of double-membrane rings (arrowhead) and horseshoe-like structures (arrow) resembling Berkeley bodies (Novick *et al*., 1980) in or near the buds where GFP-Snc1p accumulated (Figure 5B). To examine whether these structures corresponded to the GFP-Snc1p–containing compartments observed by fluorescence microscopy, we performed immunoelectron microscopic analysis for HA-Snc1p in the *cdc50-11* mutant incubated at 37°C with an anti-HA antibody by the aldehyde fixation/metaperiodate permeabilization method. We observed numerous immunogold-labeled abnormal membrane structures located in or near the bud in the *cdc50-11* mutant expressing HA-tagged Snc1p (Figure 8, D and E) but not in mutant cells expressing GFP-tagged Snc1p (our unpublished data). HA-Snc1p labeling was mostly specific for these compartments and only a minor fraction of immunogold signals was observed on other membranes. Thus, we concluded that these immunogold-positive structures were likely the same GFP-Snc1p–positive structures observed by fluorescence microscopy.

The Cdc50p–Drs2p Complex Binds to Rcy1p

Rcy1p contains an amino-terminal F-box, which interacts with Skp1p (Bai *et al*., 1996) to form a non-SCF complex, and a CAAX-box motif at its C-terminus, which mediates its interaction with membranes (Zhang and Casey 1996; Galan *et al*., 2001). Because Chen *et al*. (2005) proposed that Rcy1p functions as an effector of Ypt31p/32p in the regulation of endocytic recycling, we examined the functional relationship between the Cdc50p–Drs2p complex and Rcy1p. The *cdc50*Δ mutation exhibited synthetic lethality with a wide range of endocytosis-related mutations, including the *vrp1*Δ, *lem3*Δ (Saito *et al*., 2004), *rgp1*Δ, *ric1*Δ (Kishimoto *et al*., 2005), and *tlg2*Δ mutations (our unpublished data). Vrp1p is required for the proper organization of cortical actin patches and the internalization step during endocytosis (Munn *et al*., 1995). The Ric1p–Rgp1p complex, which acts as a GTP exchange factor for Ypt6p, and the t-SNARE Tlg2p are required for efficient fusion of endosome-derived vesicles with the Golgi (Tsukada *et al*., 1999; Lewis *et al*., 2000; Siniossoglou *et al*., 2000). The *rcy1*Δ mutation also exhibited synthetic lethality with all the mutations listed above (our unpublished data). Importantly, the *rcy1*Δ mutation did not exhibit a synthetic growth defect in combination with *cdc50*Δ; the *rcy1*Δ *cdc50*Δ mutant exhibited the same cold-sensitive growth phenotype as the *rcy1*Δ and *cdc50*Δ single mutants (our unpublished data). These genetic results suggest that *CDC50* and *RCY1* function in the same pathway.

Cooverexpression of *CDC50* and *DRS2* weakly suppressed the growth defect of the *rcy1*Δ mutant at 18°C (Figure 9A). In contrast, overexpression of *CDC50-DRS2* efficiently restored the plasma membrane localization of GFP-Snc1p in the *rcy1*Δ mutant. GFP-Snc1p was localized to the plasma membrane in only a few of the *rcy1*Δ cells (3 and 6% of the cells at 18 and 30°C, respectively), whereas when *CDC50-DRS2* was overexpressed, GFP-Snc1p was localized to polarized plasma membrane sites of the *rcy1*Δ cells to an extent comparable to that in wild-type cells (66 and 73% of the mutant cells at 18 and 30°C, respectively) (Figure 9B). Interestingly, overexpression of *GFP-SNC1* was responsible for this discrepancy; simultaneous overexpression of *GFP-SNC1* and *CDC50-DRS2* efficiently suppressed the growth defect of the *rcy1*Δ mutant, but overexpression of *GFP-SNC1* alone did not (Figure 9A). These results suggest that Cdc50p-Drs2p function downstream of the Rcy1p pathway and that Snc1p is also involved in this pathway as a functional component rather than a cargo in the endocytic recycling route.

The close functional relationship between Cdc50p-Drs2p and Rcy1p raises the possibility that these proteins are components of the same machinery. We examined whether Rcy1p colocalized with Drs2p. We constructed a strain that used a multicopy plasmid and the *RCY1* promoter to express an N-terminally GFP-tagged version of *RCY1* and the

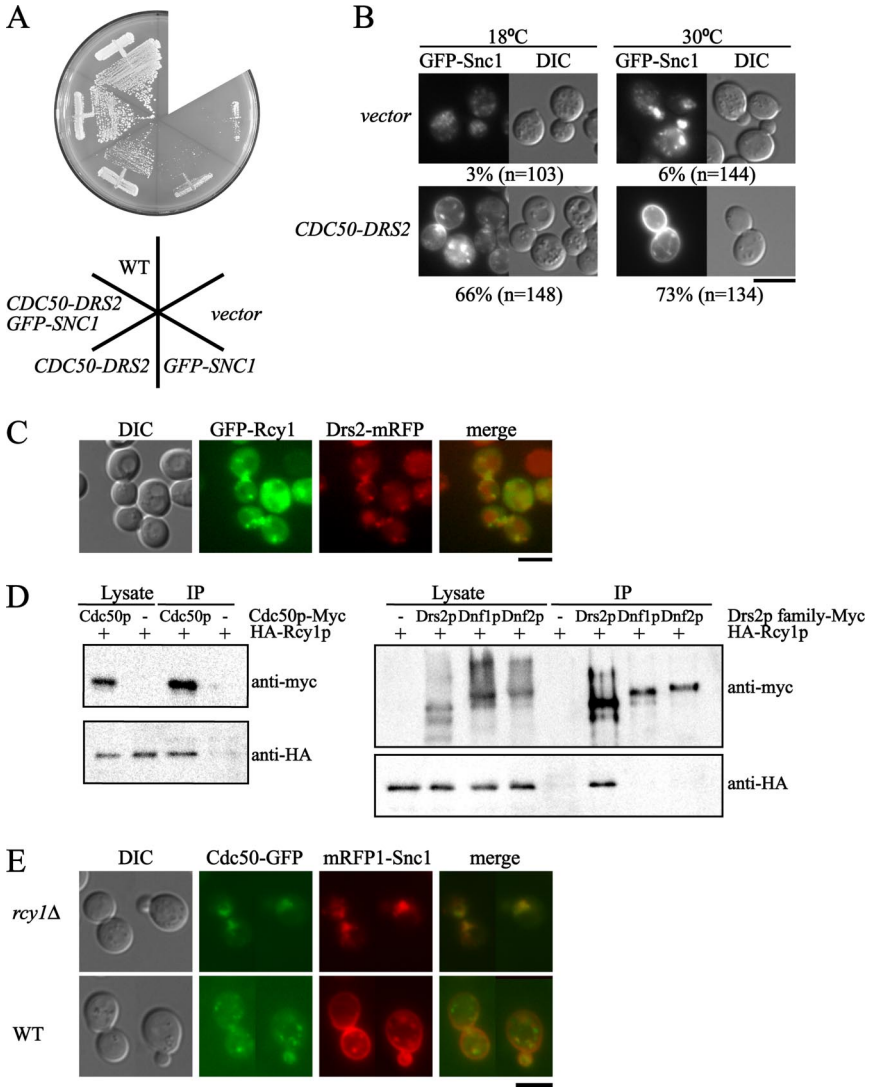

Figure 9. The Cdc50p–Drs2p complex functionally and physically interacts with Rcy1p. (A) Suppression of the growth defect of the *rcy1*Δ mutant by simultaneous overexpression of *CDC50*, *DRS2*, and *GFP-SNC1*. *rcy1*Δ mutant cells (YKT951) were cotransformed with combinations of plasmids as follows: pKT1472 (YEplac195-*DRS2-CDC50*) and pKT1490 (pRS315-*GFP-SNC1*) for *DRS2-CDC50 GFP-SNC1*, pKT1472 (YEplac195-*DRS2-CDC50*) and pRS315 for *DRS2-CDC50*, YEplac195 and pKT1490 (pRS315-*GFP-SNC1*) for *GFP-SNC1*, and YEplac195 and pRS315 for *vector*. Transformants and wild-type cells (YKT38) were streaked onto a YPDA plate, followed by incubation at 18°C for 9 d. (B) Simultaneous overexpression of *CDC50*, *DRS2*, and *GFP-SNC1* partially restored the plasma membrane localization of GFP-Snc1p in the *rcy1*Δ mutant. *rcy1*Δ mutant cells (YKT951) were cotransformed with pKT1490 (pRS315-*GFP-SNC1*) and a control vector (YEplac195; top) or pKT1472 (YEplac195-*DRS2-CDC50*; bottom). Cells were incubated at 18 or 30°C for 12 h in SD-Leu-Ura medium. Numbers indicate the percentages of cells in which GFP-Snc1p was localized to the plasma membrane. Bar, 5 μm. (C) GFP-Rcy1p partially colocalized with Drs2p-mRFP1. *DRS2-mRFP1* (YKT871) cells transformed with pKT1560 (YEplac181-*GFP-RCY1*) were grown to early to mid-logarithmic phase at 30°C in SD-Leu-Ura medium. Obtained images were merged to compare the two signal patterns. Bar, 5 μm. (D) Coimmunoprecipitation of Rcy1p with Cdc50p, Drs2p, Dnf1p, and Dnf2p. Cells grown to mid-logarithmic phase at 30°C in SDA-Ura medium. Membrane extracts were then prepared as described in *Materials and Methods*. Myc-tagged Cdc50p, Drs2p, Dnf1p, or Dnf2p were immunoprecipitated with an anti-Myc antibody from membrane extracts. Immunoprecipitates were subjected to SDS-PAGE, followed by immunoblot analysis using antibodies against Myc (top) and HA (bottom). The results shown are representative of several experiments. The yeast strains used were as follows: YKT1101 (*CDC50-Myc*) and YKT38 (*CDC50*) (left); YKT792 (*DRS2-Myc*), YKT760 (*DNF1-Myc*), YKT1062 (*DNF2-Myc*), and YKT38 (*DRS2 DNF1 DNF2*) (right). All these strains carried pKT1626 (YEplac195-*HA-BS-RCY1*). (E) Colocalization of Cdc50p-EGFP with mRFP1-Snc1p in the *rcy1*Δ mutant. *CDC50-EGFP* (YKT259) and *rcy1*Δ *CDC50-EGFP* (YKT1102) cells transformed with pKT1563 (pRS416-*mRFP1-SNC1*) were grown to mid-logarithmic phase at 30°C in SDA-Ura medium. Bar, 5 μm.

DRS2 genomic locus to express a C-terminally mRFP-tagged version of *DRS2*. Both Drs2p-mRFP1 and GFP-Rcy1p were observed in punctate structures scattered throughout the cell and partially localized to the mother-daughter neck of dividing cells (Figure 9C). Quantitative analysis of individual spots revealed that 74% of GFP-Rcy1p–positive structures were also Drs2p-mRFP1 positive (n = 270). Conversely, 49% of Drs2p-mRFP1–positive structures were also GFP-Rcy1p positive (n = 226) (Figure 9C).

To examine the physical association between Rcy1p and the Cdc50p–Drs2p complex, we performed coimmunoprecipitation experiments. We constructed a strain that used the *CDC50* genomic locus to express a C-terminally Myc-tagged version of *CDC50* and a multicopy plasmid with the own (*RCY1*) promoter to express an N-terminally HA-tagged version of *RCY1*. Cdc50p-Myc was immunoprecipitated with an anti-Myc antibody from membrane protein extracts prepared by solubilization in 1% CHAPS. The resulting immunoprecipitates were examined by immunoblot analysis with anti-Myc and anti-HA antibodies. HA-Rcy1p coimmunoprecipitated with Cdc50p-Myc (Figure 9D). HA-Rcy1p was not detected in control immunoprecipitates from cells lacking *CDC50-Myc* (Figure 9D). Similarly, we performed coimmunoprecipitation experiments using cells expressing a C-terminally Myc-tagged version of *DRS2* from the *DRS2* genomic locus and the same HA-tagged version of *RCY1*. HA-Rcy1p was detected in the Drs2p-Myc immunocomplex precipitated with an anti-Myc antibody but not in control immunoprecipitates from cells lacking *DRS2-Myc* (Figure 9D). In addition, we found that the C-terminal cytosolic region of Drs2p (amino acid positions 1216-1355) interacted with Rcy1p by the two-hybrid method (our unpublished data). In contrast, when we performed coimmunoprecipitation experiments using cells expressing a C-terminally Myc-tagged version of *DNF1* or *DNF2* from these genomic loci and the same HA-tagged version of *RCY1*, HA-Rcy1p could not be detected in the Dnf1p- and Dnf2p–Myc immunocomplexes precipitated with an anti-Myc antibody (Figure 9D). These results suggest that Rcy1p specifically interacts with the Cdc50p–Drs2p complex in vivo.

The recruitment of Rcy1p from the cytoplasm to endosomal membranes was suggested to be regulated by Ypt31p/32p (Chen *et al*., 2005), whereas like Snc1p, the Cdc50p–Drs2p complex seems to be recycled through the endocytic recycling pathway (Saito *et al*., 2004). The effect of Rcy1p depletion on the localization of Cdc50p-EGFP was examined by fluorescence microscopy. In wild-type cells at 30°C, Cdc50p-EGFP was observed as punctate structures scattered throughout the cell (Figure 9; E; Misu *et al*., 2003; Saito *et al*., 2004). In contrast, in the *rcy1*Δ mutant cells at 30°C, Cdc50p-EGFP was localized to large structures near the tip or neck of the bud, and the strength of the punctate signals concomitantly decreased (Figure 9E). These Cdc50p-EGFP–positive large structures were also labeled by mRFP1-Snc1p in the *rcy1*Δ mutant (Figure 9E). In the *rcy1*Δ mutant, 70% of mRFP1-Snc1p–positive large structures were colocalized with Cdc50p-EGFP–positive structures (n = 215), whereas 76% of the Cdc50p-EGFP–positive structures were colocalized with mRFP1-Snc1p–positive structures (n = 182). These results demonstrate that Cdc50p–Drs2p complexes accumulated in the early endosome-derived structures as Snc1p did in the *rcy1*Δ mutant (Chen *et al*., 2005). This suggests that Cdc50p-Drs2p needs to interact with Rcy1p to promote early endosome-to-TGN transport.

DISCUSSION

In the current study, we have identified *YPT31/32* as multicopy suppressors of *cdc50-ts* mutants. Because the *YPT31/32* genes were suggested to be involved in the endocytic recycling pathway as well as in the formation of post-Golgi exocytic vesicles, we examined the possible involvement of the putative PLTs in these processes. Our results suggested that the putative PLTs are involved in the endocytic recycling pathway in conjunction with Ypt31p/32p and Rcy1p, rather than in the post-Golgi exocytic pathway. Although we did not find major defects in production of high- and low-density classes of exocytic vesicles in the *sec6-4 cdc50-11* mutant, Gall *et al*. (2002) reported that *drs2* mutants exhibited defects in the formation of the high-density vesicles. This discrepancy may be attributed to the differences of methods in which high-density vesicles were detected. In Gall *et al*. (2002), the vesicles that were histochemically stained with acid phosphatase activity by EM were referred to as dense vesicles. Because the formation of these vesicles, which were induced by a *sla2* mutation or LAT-A treatment, was suppressed by *drs2-ts* mutations, they argued that Drs2p is involved in the high-density vesicle formation. However, primary defects in the *sla2* mutant cells are in endocytosis, not in exocytosis (Wendland *et al*., 1998; Engqvist-Goldstein and Drubin, 2003), and Lat-A also blocks endocytosis as well as exocytosis (Ayscough *et al*., 1997). Therefore, accumulation of acid phosphatase-containing vesicles in the *sla2* mutant may be a consequence of secondary effects due to perturbation of the endocytic pathways, making the interpretation of the effects of *drs2* mutations complicated.

Heteromeric Putative PLTs Are Required for Transport from Early Endosomes to the TGN

Similar to Cdc50p-Drs2p, Crf1p-Dnf3p may be localized to endosomal/TGN compartments, because Dnf3p-HA colocalizes with the endosome/TGN marker Kex2p (Hua *et al*., 2002) and Dnf3-HA cofractionated with endosomal/TGN membranes (Pomorski *et al*., 2003). In contrast, Lem3p-Dnf1p/2p is primarily localized to the plasma membrane, although it is also found in punctate structures that may correspond to endosomal/TGN compartments (Hua *et al*., 2002; Kato *et al*., 2002; Pomorski *et al*., 2003). We showed that Dnf1p-EGFP was primarily localized to these intracellular punctate structures in the *cdc50*Δ mutant and was exclusively localized on the plasma membrane when endocytosis was blocked, suggesting that Lem3p-Dnf1p/2p is recycled by the endocytic pathway (Saito *et al*., 2004). Lem3p-Dnf1p/2p may cooperate with Cdc50p-Drs2p at early endosomes for endocytic recycling. If this is the case, what is the function of Lem3p-Dnf1p/2p when it is localized at the plasma membrane? Interestingly, the *lem3*Δ and *dnf1*Δ *dnf2*Δ *dnf3*Δ mutants display elongated cell morphologies at lower temperatures (Hua *et al*., 2002; Saito, K., Fujimura-Kamada, K., and Tanaka, K., unpublished observations), suggesting that Lem3p-Dnf1p/2p may be involved in the negative regulation of polarized cell growth. In contrast to the depolarized organization of the actin cytoskeleton in the *cdc50*Δ mutant at 18°C (Misu *et al*., 2003), the *cdc50-ts* mutants exhibited polarized organization of the actin cytoskeleton at 37°C, possibly due to the effect of the *lem3*Δ mutation (our unpublished data).

The Snc1p-containing large membranous structures that accumulated in the *cdc50-ts* mutants seem to be of endocytic origin, suggesting that the *cdc50-ts* mutants are defective in the formation of vesicles from early endosomes. The Rab family small GTPase Ypt6p and its nucleotide exchange factor consisting of Ric1p and Rgp1p are also required for endocytic recycling (Siniossoglou *et al*., 2000; Siniossoglou and Pelham, 2001). These factors are localized to the TGN to assist fusion between endosomally derived vesicles and the TGN. Both Ric1p-EGFP and Rgp1p-EGFP exhibited normal punctate localization patterns in the *cdc50-ts* mutants (our unpublished data), suggesting that the fusion step of endocytic vesicles with the TGN is not severely affected in the *cdc50-ts* mutants. Synthetic growth defects observed with combinations of the *cdc50*Δ mutation and the *ric1*Δ, *rgp1*Δ, and *ypt6* mutations (Kishimoto *et al*., 2005) may be due to multiple defects in different steps of the endocytic recycling pathway.

One possible explanation for accumulation of early endosomal structures is that proteins required for the formation of vesicles destined for the TGN are not normally transported from the TGN to early endosomes in the *cdc50-ts* mutants. Tlg1p, which is thought to be recycled between early endosomes and the TGN (Lewis *et al*., 2000), however, accumulated in the Snc1p-containing structures, suggesting that the TGN-to-early endosome pathway was not impaired. Mislocalization of Kex2p in *drs2* mutants was explained by defective transport from the TGN (Chen *et al*., 1999), but it is also possible that Kex2p was transported to vacuoles by default due to defective retrieval from the early endosome to the TGN as suggested previously (Wilcox *et al*., 1992; Holthuis *et al*., 1998; Spelbrink and Nothwehr, 1999).

One intriguing possibility is that the putative PLTs are directly involved in vesicle formation at early endosomes. A proposed role for PLTs is that they locally generate phospholipid asymmetry to assist membrane deformation during vesicle budding or to recruit proteins that promote vesicle formation (Graham, 2004). It was previously suggested that Drs2p is involved in Arf1p- and clathrin-dependent vesicle formation; *DRS2* was originally identified because a mutant allele was synthetically lethal with *arf1*Δ (Chen and Graham, 1998; Chen *et al*., 1999), and significantly fewer clathrin-coated vesicles were isolated from *drs2*Δ cells than from wild-type cells (Chen *et al*., 1999). Thus, the accumulation of early endosomal structures in the *cdc50-ts* mutants may be due to defective formation of clathrin-coated vesi-

cles. Involvement of clathrin in the endocytic recycling pathway has been demonstrated in mammalian cells (van Dam and Stoorvogel, 2002) and suggested in yeast; clathrin, and clathrin adaptor complex 1 act to recycle chitin synthase III (Chs3p) from the early endosome to the TGN (Valdivia *et al*., 2002).

Functional Relationship between Putative PLTs and the Ypt31p/32p–Rcy1p Pathway

Results from our group and other groups suggest that *RCY1* is functionally equivalent to *CDC50*. Immuno-EM suggested that the *rcy1*Δ mutant also accumulates large membranous structures that contain Tlg1p (Wiederkehr *et al*., 2000). In addition to defects in endocytic recycling, the *cdc50*Δ and *rcy1*Δ mutants share a number of other phenotypes, including cold sensitivity of growth, minimum defects in secretion, and vacuolar protein sorting (Wiederkehr *et al*., 2000), and intracellular assembly of cortical actin patches (Kishimoto *et al*., 2005; Kishimoto, K., Yamamoto, T., and Tanaka, K., unpublished observations). Growth defects of the *cdc50*Δ mutant were not exacerbated by *rcy1*Δ, whereas *rcy1*Δ as well as *cdc50*Δ resulted in synthetic growth defects when combined the *lem3*Δ mutation. These results, taken together with the coimmunoprecipitation of Rcy1p with Cdc50p as well as with Drs2p, suggest that Rcy1p plays an important role in regulation or function of the Cdc50p–Drs2p putative PLT. We favor an upstream regulatory role for Ypt31p/32p-Rcy1p based on the following observations. Simultaneous overexpression of *CDC50*, *DRS2*, and *GFP-SNC1* efficiently restored growth and endocytic recycling of GFP-Snc1p in the *rcy1*Δ mutant, whereas overexpression of *YPT31/32* only weakly suppressed defects in growth and endocytic recycling of GFP-Snc1p in the *cdc50-ts* mutants. In addition, overexpression of *YPT31/32* did not suppress the cold-sensitive growth defect of the *cdc50*Δ mutant, suggesting that a residual activity of Cdc50p-Drs2p is required for the suppression.

Genetic studies suggested that transport protein particle (TRAPP) II, a large complex that mediates membrane traffic, functions upstream of *YPT31* (Wang and Ferro-Novick, 2002; Yamamoto and Jigami, 2002; Sciorra *et al*., 2005). An allele of *TRS130* encoding a subunit of TRAPP II was identified as a synthetic lethal mutation with *arf1*Δ (Zhang *et al*., 2002). This *trs130-101 arf1*Δ mutant did not exhibit defects in either CPY processing or invertase secretion, and overexpression of *YPT31/32* suppressed the growth defects of the *trs130-101 arf1*Δ mutant. Interestingly, it was recently reported that mutants in another component of TRAPP II, *TRS120*, exhibited defects in the endocytic recycling of Snc1p, but not in general secretion (Cai *et al*., 2005). In the *trs120* mutant, aberrant and large membrane structures accumulated, reminiscent of the membrane structures observed in the *cdc50-ts* mutants. Although it is controversial whether TRAPP II is a GDP/GTP exchange factor for Ypt31p/32p (Jones *et al*., 2000; Wang and Ferro-Novick, 2002), TRAPP II may activate Ypt31p/32p to promote vesicle formation from early endosomes.

Localization of Rcy1p to internal membranes was not affected by blockade of endocytic internalization (our unpublished data), whereas the *ypt31*Δ *ypt32-ts* mutations caused diffuse GFP–Rcy1p labeling in the cytoplasm (Chen *et al*., 2005). Thus, Ypt31p/32p may regulate recruitment of Rcy1p to endosomal membranes by stimulating the interaction of Rcy1p with Cdc50p-Drs2p on endosomal membranes. Cdc50p-Drs2p, however, is not likely to be the sole receptor for Rcy1p, because GFP-Rcy1p was still localized to internal punctate structures in the *cdc50-ts* mutants at 37°C (our unpublished observations). Because Rcy1p also binds to Snc1p (Chen *et al*., 2005), Ypt31p/32p-GTP-Rcy1p might recruit and couple putative PLTs with cargo proteins on early endosomal membranes. Interestingly, efficient suppression of defects in growth and endocytic recycling in the *rcy1*Δ mutant by overexpression of *CDC50* and *DRS2* also required the overexpression of *GFP-SNC1*. Formation of a functional complex consisting of Rcy1p, Snc1p, and Cdc50p-Drs2p may lead to utilization of the activity of putative PLTs to promote subsequent processes for vesicle budding.

ACKNOWLEDGMENTS

We thank Drs. Charles Boone, Michael Lewis, Hugh Pelham, Roger Tsien, Yoshinori Ohsumi, Yoshikazu Ohya, Masato Umeda, Akihiko Nakano, and Ramon Serrano for yeast strains, plasmids, and antibodies; and Dr. Masahiko Watanabe for use of the microtome. We thank our colleagues in the Tanaka laboratory for valuable discussions. We also thank Eriko Itoh for technical assistance. This work was supported by grants-in-aid for scientific research from the Japan Society for the Promotion of Science and the Ministry of Education, Culture, Sports, Science and Technology of Japan (to K.F.-K., K.S., T.Y., and K.T.).

REFERENCES

Alder-Baerens, N., Lisman, Q., Luong, L., Pomorski, T., and Holthuis, J. C. (2006). Loss of P4 ATPases Drs2p and Dnf3p disrupts aminophospholipid transport and asymmetry in yeast post-Golgi secretory vesicles. Mol. Biol. Cell *17*, 1632–1642.

Ayscough, K. R., Stryker, J., Pokala, N., Sanders, M., Crews, P., and Drubin, D. G. (1997). High rates of actin filament turnover in budding yeast and roles for actin in establishment and maintenance of cell polarity revealed using the actin inhibitor latrunculin-A. J. Cell Biol. *137*, 399–416.

Bai, C., Sen, P., Hofmann, K., Ma, L., Goebl, M., Harper, J. W., and Elledge, S. J. (1996). *SKP1* connects cell cycle regulators to the ubiquitin proteolysis machinery through a novel motif, the F-box. Cell *86*, 263–274.

Benli, M., Doring, F., Robinson, D. G., Yang, X., and Gallwitz, D. (1996). Two GTPase isoforms, Ypt31p and Ypt32p, are essential for Golgi function in yeast. EMBO. J. *15*, 6460–6475.

Black, M. W., and Pelham, H. R. (2000). A selective transport route from Golgi to late endosomes that requires the yeast GGA proteins. J. Cell Biol. *151*, 587–600.

Brickner, J. H., and Fuller, R. S. (1997). *SOI1* encodes a novel, conserved protein that promotes TGN-endosomal cycling of Kex2p and other membrane proteins by modulating the function of two TGN localization signals. J. Cell Biol. 139, 23–36.

Cai, H., Zhang, Y., Pypaert, M., Walker, L., and Ferro-Novick, S. (2005). Mutants in *trs120* disrupt traffic from the early endosome to the late Golgi. J. Cell Biol. *171*, 823–833.

Catty, P., de Kerchove d'Exaerde, A., and Goffeau, A. (1997). The complete inventory of the yeast *Saccharomyces cerevisiae* P-type transport ATPases. FEBS Lett. *409*, 325–332.

Cereghino, J. L., Marcusson, E. G., and Emr, S. D. (1995). The cytoplasmic tail domain of the vacuolar protein sorting receptor Vps10p and a subset of VPS gene products regulate receptor stability, function, and localization. Mol. Biol. Cell *6*, 1089–1102.

Chen, C. Y., and Graham, T. R. (1998). An *arf1*Δ synthetic lethal screen identifies a new clathrin heavy chain conditional allele that perturbs vacuolar protein transport in *Saccharomyces cerevisiae*. Genetics *150*, 577–589.

Chen, C. Y., Ingram, M. F., Rosal, P. H., and Graham, T. R. (1999). Role for Drs2p, a P-type ATPase and potential aminophospholipid translocase, in yeast late Golgi function. J. Cell Biol. *147*, 1223–1236.

Chen, S. H., Chen, S., Tokarev, A. A., Liu, F., Jedd, G., and Segev, N. (2005). Ypt31/32 GTPases and their novel F-box effector protein Rcy1 regulate protein recycling. Mol. Biol. Cell *16*, 178–192.

Conibear, E., and Stevens, T. H. (2000). Vps52p, Vps53p, and Vps54p form a novel multisubunit complex required for protein sorting at the yeast late Golgi. Mol. Biol. Cell *11*, 305–323.

Cooper, A. A., and Stevens, T. H. (1996). Vps10p cycles between the late-Golgi and prevacuolar compartments in its function as the sorting receptor for multiple yeast vacuolar hydrolases. J. Cell Biol. *133*, 529–541.

David, D., Sundarababu, S., and Gerst, J. E. (1998). Involvement of long chain fatty acid elongation in the trafficking of secretory vesicles in yeast. J. Cell Biol. *143*, 1167–1182.

Elble, R. (1992). A simple and efficient procedure for transformation of yeasts. Biotechniques *13*, 18–20.

Engqvist-Goldstein, A. E., and Drubin, D. G. (2003). Actin assembly and endocytosis: from yeast to mammals. Annu. Rev. Cell Dev. Biol. *19*, 287–332.

Franzusoff, A., Redding, K., Crosby, J., Fuller, R. S., and Schekman, R. (1991). Localization of components involved in protein transport and processing through the yeast Golgi apparatus. J. Cell Biol. *112*, 27–37.

Galan, J. M., Wiederkehr, A., Seol, J. H., Haguenauer-Tsapis, R., Deshaies, R. J., Riezman, H., and Peter, M. (2001). Skp1p and the F-box protein Rcy1p form a non-SCF complex involved in recycling of the SNARE Snc1p in yeast. Mol. Cell. Biol. *21*, 3105–3117.

Gall, W. E., Geething, N. C., Hua, Z., Ingram, M. F., Liu, K., Chen, S. I., and Graham, T. R. (2002). Drs2p-dependent formation of exocytic clathrin-coated vesicles *in vivo*. Curr. Biol. *12*, 1623–1627.

Gaynor, E. C., te Heesen, S., Graham, T. R., Aebi, M., and Emr, S. D. (1994). Signal-mediated retrieval of a membrane protein from the Golgi to the ER in yeast. J. Cell Biol. *127*, 653–665.

Gietz, R. D., and Sugino, A. (1988). New yeast-*Escherichia coli* shuttle vectors constructed with *in vitro* mutagenized yeast genes lacking six-base pair restriction sites. Gene *74*, 527–534.

Gietz, R. D., and Woods, R. A. (2002). Transformation of yeast by lithium acetate/single-stranded carrier DNA/polyethylene glycol method. Methods Enzymol. *350*, 87–96.

Goldstein, A. L., and McCusker, J. H. (1999). Three new dominant drug resistance cassettes for gene disruption in *Saccharomyces cerevisiae*. Yeast *15*, 1541–1553.

Graham, T. R. (2004). Flippases and vesicle-mediated protein transport. Trends Cell Biol. *14*, 670–677.

Gurunathan, S., David, D., and Gerst, J. E. (2002). Dynamin and clathrin are required for the biogenesis of a distinct class of secretory vesicles in yeast. EMBO J. *21*, 602–614.

Guthrie, C., and, Fink, G. R. (1991). Guide to Yeast Genetics and Molecular Biology, San Diego, CA: Academic Press.

Harsay, E., and Bretscher, A. (1995). Parallel secretory pathways to the cell surface in yeast. J. Cell Biol. *131*, 297–310.

Holthuis, J. C., Nichols, B. J., Dhruvakumar, S., and Pelham, H. R. (1998). Two syntaxin homologues in the TGN/endosomal system of yeast. EMBO J. *17*, 113–126.

Holthuis, J. C., and Levine, T. P. (2005). Lipid traffic: floppy drives and a superhighway. Nat. Rev. Mol. Cell Biol. *6*, 209–220.

Hua, Z., Fatheddin, P., and Graham, T. R. (2002). An essential subfamily of Drs2p-related P-type ATPases is required for protein trafficking between Golgi complex and endosomal/vacuolar system. Mol. Biol. Cell *13*, 3162–3177.

Jedd, G., Mulholland, J., and Segev, N. (1997). Two new Ypt GTPases are required for exit from the yeast *trans*-Golgi compartment. J. Cell Biol. *137*, 563–580.

Jones, S., Newman, C., Liu, F., and Segev, N. (2000). The TRAPP complex is a nucleotide exchanger for Ypt1 and Ypt31/32. Mol. Biol. Cell *11*, 4403–4411.

Kaiser, C. A., and Schekman, R. (1990). Distinct sets of *SEC* genes govern transport vesicle formation and fusion early in the secretory pathway. Cell *61*, 723–733.

Kato, U., Emoto, K., Fredriksson, C., Nakamura, H., Ohta, A., Kobayashi, T., Murakami-Murofushi, K., Kobayashi, T., and Umeda, M. (2002). A. novel membrane protein, Ros3p, is required for phospholipid translocation across the plasma membrane in *Saccharomyces cerevisiae*. J. Biol. Chem. *277*, 37855–37862.

Kihara, A., Noda, T., Ishihara, N., and Ohsumi, Y. (2001). Two distinct Vps34 phosphatidylinositol3-kinase complexes function in autophagy and carboxypeptidase Y. sorting in *Saccharomyces cerevisiae*. J. Cell Biol. *152*, 519–530.

Kishimoto, T., Yamamoto, T., and Tanaka, K. (2005). Defects in structural integrity of ergosterol and the Cdc50p-Drs2p putative phospholipid translocase cause accumulation of endocytic membranes, onto which actin patches are assembled in yeast. Mol. Biol. Cell *16*, 5592–5609.

Lewis, M. J., Nichols, B. J., Prescianotto-Baschong, C., Riezman, H., and Pelham, H. R. (2000). Specific retrieval of the exocytic SNARE Snc1p from early yeast endosomes. Mol. Biol. Cell *11*, 23–38.

Longtine, M. S., McKenzie, A. 3rd, Demarini, D. J., Shah, N. G., Wach, A., Brachat, A., Philippsen, P., and Pringle, J. R. (1998). Additional modules for versatile and economical PCR-based gene deletion and modification in *Saccharomyces cerevisiae*. Yeast *14*, 953–961.

Misu, K., Fujimura-Kamada, K., Ueda, T., Nakano, A., Katoh, H., and Tanaka, K. (2003). Cdc50p, a conserved endosomal membrane protein, controls polarized growth in *Saccharomyces cerevisiae*. Mol. Biol. Cell *14*, 730–747.

Mulholland, J., and Botstein, D. (2002). Immunoelectron microscopy of aldehyde-fixed yeast cells. Methods Enzymol. *351*, 50–81.

Munn, A. L., Stevenson, B. J., Geli, M. I., and Riezman, H. (1995). *end5*, *end6*, and *end7*, mutations that cause actin delocalization and block the internalization step of endocytosis in *Saccharomyces cerevisiae*. Mol. Biol. Cell *6*, 1721–1742.

Natarajan, P., Wang, J., Hua, Z., and Graham, T. R. (2004). Drs2p-coupled aminophospholipid translocase activity in yeast Golgi membranes and relationship to *in vivo* function. Proc. Natl. Acad. Sci. USA *101*, 10614–10619.

Novick, P., Field, C., and Schekman, R. (1980). Identification of 23 complementation groups required for post-translational events in the yeast secretory pathway. Cell *21*, 205–215.

Ortiz, D., Medkova, M., Walch-Solimena, C., and Novick, P. (2002). Ypt32 recruits the Sec4p guanine nucleotide exchange factor, Sec2p, to secretory vesicles; evidence for a Rab cascade in yeast. J. Cell Biol. *157*, 1005–1015.

Pomorski, T., Lombardi, R., Riezman, H., Devaux, P. F., van Meer, G., and Holthuis, J. C. (2003). Drs2p-related P-type ATPases Dnf1p and Dnf2p are required for phospholipid translocation across the yeast plasma membrane and serve a role in endocytosis. Mol. Biol. Cell *14*, 1240–1254.

Pomorski, T., Holthuis, J. C., Herrmann, A., and van Meer, G. (2004). Tracking down lipid flippases and their biological functions. J. Cell Sci. *117*, 805–813.

Raymond, C. K., Howald-Stevenson, I., Vater, C. A., and Stevens, T. H. (1992). Morphological classification of the yeast vacuolar protein sorting mutants: evidence for a prevacuolar compartment in class E *vps* mutants. Mol. Biol. Cell *3*, 1389–1402.

Roberts, C. J., Raymond, C. K., Yamashiro, C. T., and Stevens, T. H. (1991). Methods for studying the yeast vacuole. Methods Enzymol. *194*, 644–661.

Rose, M. D., Winston, F., and Hieter, and P. (1990). Methods in Yeast Genetics: A Laboratory Course Manual, Cold Spring Harbor, NY: Cold Spring Harbor Laboratory Press.

Rothblatt, J., and Schekman, R. (1989). A. hitchhiker's guide to analysis of the secretory pathway in yeast. Methods Cell Biol. *32*, 3–36.

Rubin, G. M. (1973). The nucleotide sequence of *Saccharomyces cerevisiae* 5.8 S ribosomal ribonucleic acid. J. Biol. Chem. *248*, 3860–3875.

Saito, K., Fujimura-Kamada, K., Furuta, N., Kato, U., Umeda, M., and Tanaka, K. (2004). Cdc50p, a protein required for polarized growth, associates with the Drs2p P-type ATPase implicated in phospholipid translocation in *Saccharomyces cerevisiae*. Mol. Biol. Cell *15*, 3418–3432.

Sciorra, V. A., Audhya, A., Parsons, A. B., Segev, N., Boone, C., and Emr, S. D. (2005). Synthetic genetic array analysis of the PtdIns 4-kinase Pik1p identifies components in a Golgi-specific Ypt31/rab-GTPase signaling pathway. Mol. Biol. Cell *16*, 776–793.

Seaman, M. N., Marcusson, E. G., Cereghino, J. L., and Emr, S. D. (1997). Endosome to Golgi retrieval of the vacuolar protein sorting receptor, Vps10p, requires the function of the *VPS29*, *VPS30*, and *VPS35* gene products. J. Cell Biol. *137*, 79–92.

Sikorski, R. S., and Hieter, P. (1989). A. system of shuttle vectors and yeast host strains designed for efficient manipulation of DNA in *Saccharomyces cerevisiae*. Genetics *122*, 19–27.

Siniossoglou, S., Peak-Chew, S. Y., and Pelham, H. R. (2000). Ric1p and Rgp1p form a complex that catalyses nucleotide exchange on Ypt6p. EMBO J. *19*, 4885–4894.

Siniossoglou, S., and Pelham, H. R. (2001). An effector of Ypt6p binds the SNARE Tlg1p and mediates selective fusion of vesicles with late Golgi membranes. EMBO J. *20*, 5991–5998.

Spelbrink, R. G., and Nothwehr, S. F. (1999). The yeast *GRD20* gene is required for protein sorting in the *trans*-Golgi network/endosomal system and for polarization of the actin cytoskeleton. Mol. Biol. Cell *10*, 4263–4281.

Stevens, T., Esmon, B., and Schekman, R. (1982). Early stages in the yeast secretory pathway are required for transport of carboxypeptidase Y to the vacuole. Cell *30*, 439–448.

Toi, H., Fujimura-Kamada, K., Irie, K., Takai, Y., Todo, S., and Tanaka, K. (2003). She4p/Dim1p interacts with the motor domain of unconventional myosins in the budding yeast, *Saccharomyces cerevisiae*. Mol. Biol. Cell *14*, 2237–2249.

Tsukada, M., Will, E., and Gallwitz, D. (1999). Structural and functional analysis of a novel coiled-coil protein involved in Ypt6 GTPase-regulated protein transport in yeast. Mol. Biol. Cell *10*, 63–75.

Valdivia, R. H., Baggott, D., Chuang, J. S., and Schekman, R. W. (2002). The yeast clathrin adaptor protein complex 1 is required for the efficient retention of a subset of late Golgi membrane proteins. Dev. Cell *2*, 283–294.

van Dam, E. M., and Stoorvogel, W. (2002). Dynamin-dependent transferrin receptor recycling by endosome-derived clathrin-coated vesicles. Mol. Biol. Cell *13*, 169–182.

Vida, T. A., and Emr, S. D. (1995). A. new vital stain for visualizing vacuolar membrane dynamics and endocytosis in yeast. J. Cell Biol. *128*, 779–792.

Wang, W., and Ferro-Novick, S. (2002). A Ypt32p exchange factor is a putative effector of Ypt1p. Mol. Biol. Cell *13*, 3336–3343.

Wendland, B., Emr, S. D., and Riezman, H. (1998). Protein traffic in the yeast endocytic and vacuolar protein sorting pathways. Curr. Opin. Cell Biol. *10*, 513–522.

Wiederkehr, A., Avaro, S., Prescianotto-Baschong, C., Haguenauer-Tsapis, R., and Riezman, H. (2000). The F-box protein Rcy1p is involved in endocytic membrane traffic and recycling out of an early endosome in *Saccharomyces cerevisiae*. J. Cell Biol. *149*, 397–410.

Wilcox, C. A., Redding, K., Wright, R., and Fuller, R. S. (1992). Mutation of a tyrosine localization signal in the cytosolic tail of yeast Kex2 protease disrupts Golgi retention and results in default transport to the vacuole. Mol. Biol. Cell *3*, 1353–1371.

Yahara, N., Ueda, T., Sato, K., and Nakano, A. (2001). Multiple roles of Arf1 GTPase in the yeast exocytic and endocytic pathways. Mol. Biol. Cell *12*, 221–238.

Yamamoto, K., and Jigami, Y. (2002). Mutation of *TRS130*, which encodes a component of the TRAPPII complex, activates transcription of *OCH1* in *Saccharomyces cerevisiae*. Curr. Genet. *42*, 85–93.

Zhang, C. J., Bowzard, J. B., Greene, M., Anido, A., Stearns, K., and Kahn, R. A. (2002). Genetic interactions link *ARF1*, *YPT31/32* and *TRS130*. Yeast *19*, 1075–1086.

Zhang, F. L., and Casey, P. J. (1996). Protein prenylation: molecular mechanisms and functional consequences. Annu. Rev. Biochem. *65*, 241–269.